Czech Technical University in Prague

Faculty of Electrical Engineering
Department of Electric Drives and Traction

CONTROL STRATEGY OF MULTILEVEL CONVERTERS FOR VARIABLE SPEED DRIVES

Master's thesis

Norbert Kanaloš

Supervisor: Ing. Pavel Kobrle, Ph.D.

Prague, August 2022

ZADÁNÍ DIPLOMOVÉ PRÁCE

I. OSOBNÍ A STUDIJNÍ ÚDAJE

Příjmení: **Kanaloš** Jméno: **Norbert** Osobní číslo: **465908**

Fakulta/ústav: **Fakulta elektrotechnická**

Zadávající katedra/ústav: **Katedra elektrických pohonů a trakce**

Studijní program: **Elektrotechnika, energetika a management**

Specializace: **Elektrické pohony**

II. ÚDAJE K DIPLOMOVÉ PRÁCI

Název diplomové práce:

Řídicí strategie víceúrovňových měničů pro aplikace v elektrických pohonech

Název diplomové práce anglicky:

Control Strategy of Multilevel Converters for Variable Speed Drives

Pokyny pro vypracování:

1) Seznamte se s možnostmi řízení víceúrovňových měničů pro elektrické pohony.
2) Vytvořte vhodný simulační model měniče.
3) Pro zhotovený model měniče vytvořte vhodnou strategii řízení.
4) Proveďte simulace k ověření správnosti řízení a dosažené výsledky relevantně zhodnoťte.

Seznam doporučené literatury:

[1] Cui, S., Jung, J., Lee, Y. and Sul, S.: A novel control strategy of a modular multilevel converter (MMC) based VSC-HVDC transmission system, 2015 IEEE Applied Power Electronics Conference and Exposition (APEC), Charlotte, NC, 2015, pp. 972-979.
[2] Adam, G. P., Abdelsalam, I., Fletcher, J. E., Burt, G. M., Holliday, D. and Finney, S. J.: New Efficient Submodule for a Modular Multilevel Converter in Multiterminal HVDC Networks, IEEE Transactions on Power Electronics, vol. 32, no. 6, pp. 4258-4278, June 2017.
[3] McGrath, B. P., Teixeira, C. A. and Holmes, D. G.: Optimized Phase Disposition (PD) Modulation of a Modular Multilevel Converter, IEEE Transactions on Industry Applications, vol. 53, no. 5, pp. 4624-4633, Sept.-Oct. 2017.
[4] Dahmen, C. and Marquardt R., Progress of High Power Multilevel Converters: Combining Silicon and Silicon Carbide, PCIM Europe 2017; International Exhibition and Conference for Power Electronics, Intelligent Motion, Renewable Energy and Energy Management, Nuremberg, Germany, 2017, pp. 1-7.

Jméno a pracoviště vedoucí(ho) diplomové práce:

Ing. Pavel Kobrle, Ph.D. katedra elektrických pohonů a trakce

Jméno a pracoviště druhé(ho) vedoucí(ho) nebo konzultanta(ky) diplomové práce:

Datum zadání diplomové práce: **11.02.2022** Termín odevzdání diplomové práce: **15.08.2022**

Platnost zadání diplomové práce: **30.09.2023**

Ing. Pavel Kobrle, Ph.D. podpis vedoucí(ho) práce	podpis vedoucí(ho) ústavu/katedry	prof. Mgr. Petr Páta, Ph.D. podpis děkana(ky)

III. PŘEVZETÍ ZADÁNÍ

Diplomant bere na vědomí, že je povinen vypracovat diplomovou práci samostatně, bez cizí pomoci, s výjimkou poskytnutých konzultací. Seznam použité literatury, jiných pramenů a jmen konzultantů je třeba uvést v diplomové práci.

.	
Datum převzetí zadání	Podpis studenta

Declaration

I hereby declare that the presented thesis is my own work and that I have cited all sources of information in accordance with the Guideline for adhering to ethical principles when elaborating an academic final thesis.

Prague, ...

Signature

Acknowledgement

I would like to express my gratitude to my supervisor Ing. Pavlovi Kobrlemu, Ph.D., for his guidance, advice and patience throughout the course of this work.

I would also like express my sincere thanks to my family and friends for their continuous support and help during my studies.

Abstract

This thesis is focused on the control strategy of the three-level neutral point clamped converter for variable speed drives and is divided into 2 parts.

In the theoretical part are presented the conventional typologies of two-level and multilevel converters and modulation techniques that are used to control their output voltage. Further, the mathematical model of the induction motor and reference frames are derived, together with the control strategy of the induction motor. Finally, the struggles of controlling the variable frequency drives are described.

The objective of the practical part is to make a functional model of the three-level converter and appropriate control strategy. The simulation model is made in the MATLAB Simulink environment with the use of Simscape library. The conducted simulations are then compared and evaluated.

Key words

Variable speed drives, three-level converter, neutral point clamped converter, induction motor, pulse width modulation, space vector modulation, MATLAB, Simulink

Table of Contents

List of Figures

Nomenclature

Abbreviations

AC	Alternating Current
ANPC	Active Neutral Point Clamped
APOD	Alternative Phase Opposition Disposition
D	Diode
DC	Direct Current
DTC	Direct Torque Control
FC	Flying Capacitor
FOC	Field Oriented Control
IEGT	Injection Enhanced Gate Transistor
IGBT	Insulated Gate Bipolar Transistor
IGCT	Insulated Gate-Commutated Thyristor
IM	Induction Motor
MC	Multilevel Converter
MMC	Modular Multilevel Converter
S	Switching cell
SiC MOSFET	Silicon Carbide Metal–Oxide–Semiconductor Field-Effect Transistor
NPC	Neutral Point Clamped
NTV	Nearest Three Vector
ODE	Ordinary Differential Equation
PD	Phase Disposition
POD	Phase Opposition Disposition
PWM	Pulse Width Modulation
SGCT	Symmetric Gate-Commutated Thyristor
SM	Submodule
SPWM	Sinusoidal Pulse Width Modulation
SVM	Space Vector Modulation
SVPWM	Space Vector Pulse Width Modulation
VSD	Variable Speed Drive

Symbols

0, P, N	Zero, positive, negative output voltage
A_c, A_r	Carrier, reference signal amplitude
B	Friction coefficient
f, f_c, f_r	Supply, carrier signal, reference signal frequency
$\bar{I}_r, \bar{I}_s$	Vector of rotor, stator current
i_n	Neutral current
i_r, i_s	Instantaneous rotor, stator current

$i_{r\alpha}, i_{r\beta}, i_{s\alpha}, i_{s\beta}$	α, β components of the rotor, stator current
$i_{rd}, i_{rq}, i_{sd}, i_{sq}$	d, q components of the rotor, stator current
$i_{rd_r}, i_{rq_r}, i_{sd_r}, i_{sq_r}$	d_r, q_r components of the rotor, stator current
J	Moment of inertia
L_m, L_r, L_s	Mutual, rotor, stator inductance
M	Modulation index
n	Neutral point
P	Frequency ratio
p_p	Number of pole pairs
R_r, R_s	Rotor, stator resistance
T_0, T_1, T_2	Dwell times
T_e, T_l	Electromagnetic, load torque
T_s	Switching period
V_{DC}	DC-link voltage
V_a, V_b, V_c, V_{ln}	phase A, phase B, phase C, line-to-neutral voltage
$\bar{V}_0 - \bar{V}_{18}, V_a, V_b$	Space vector
$\bar{V}_\alpha, \bar{V}_\beta$	α, β components of the space vector voltage
$\bar{V}_{ref}$	Reference space vector
$\bar{V}_r, \bar{V}_s$	Vector of rotor, stator voltage
$v_{r\alpha}, v_{r\beta}, v_{s\alpha}, v_{s\beta}$	α, β components of the rotor, stator voltage
$v_{rd}, v_{rq}, v_{sd}, v_{sq}$	d, q components of the rotor, stator voltage
$v_{rd_r}, v_{rq_r}, v_{sd_r}, v_{sq_r}$	d_r, q_r components of the rotor, stator voltage
σ	Leakage factor
φ	Phase angle
$\bar{\Psi}_r, \bar{\Psi}_s$	Rotor, stator magnetic flux
ψ_r, ψ_s	Instantaneous rotor, stator magnetic flux
$\psi_{r\alpha}, \psi_{r\beta}, \psi_{s\alpha}, \psi_{s\beta}$	α, β components of the rotor, stator magnetic flux
$\psi_{rd}, \psi_{rq}, \psi_{sd}, \psi_{sq}$	d, q components of the rotor, stator magnetic flux
$\psi_{rd_r}, \psi_{rq_r}, \psi_{sd_r}, \psi_{sq_r}$	d_r, q_r components of the rotor, stator magnetic flux
$\omega, \omega_c, \omega_r, \omega_s, \omega_{sl}$	Mechanical, arbitrary reference frame, rotor, synchronous, slip angular speed

1 Introduction

The basic function of a Variable Speed Drive (VSD) is to regulate the speed and rotational force, or output torque of mechanical equipment. The supply powers the drive, which regulates the power being fed to the motor. At first, the AC power is converted into DC power in a rectifier. The DC power is then fed into the DC control section, consisting of capacitors and inductors. Together they work as a filter and help smooth out the electrical waveform. After that, the DC power is inverted into AC power and is being fed into the motor [1], [2], [3].

Typically, motors are being chosen based on the load, to provide the maximal required output power. For maximum designed loads, motors run at the maximum constant speed and the power input to the motor is constant. However, if the load is reduced, matching the rotor speed to the load requirement saves significant amount of energy. Modern electrical VSDs can independently of load maintain the speed of a motor to accuracy of ±0.1 % [2].

There are many motors used in industries or offices that need to be retrofitted because they run inefficiently. Using VSDs instead of a motors supplied directly from the grid, can increase efficiency of motors by allowing them to operate at the ideal speed. In many applications VSDs can decrease the consumption by 60 %. Use of VSD decreases energy consumption, increases energy efficiency, prolongs the life of the equipment and improves power factor. This helps the owner to reduce the costs of operation [2].

The VSDs used for such operations are typically indirect converters, that have a DC-link between the AC input and AC output. Depending on the motor, which is being supplied, the VSDs can be divided by their maximal output voltage, number of voltage levels, topology, or control method. For high voltage motors, the multilevel converters are most suitable. More voltage levels put less stress on the electrical parts, which allows the use of conventional electrical parts instead of specialized parts. Although it is theoretically possible to have as many voltage levels as one pleases, control methods get more complicated with every additional level.

Control methods can be chosen either specifically for the motor or can be chosen based on general performance. The most popular methods are Pulse Width Modulation (PWM) and Space Vector Modulation (SVM), mainly because of their relative simplicity and possibility to control the harmonics in the output voltage.

Because the DC-link includes capacitors, some balancing method is usually implemented. Every converter's topology has its own balancing technique, that helps to stabilize the DC voltage and prevent the voltage of the capacitors to deviate from each other. Excluding the voltage balancing of the capacitors in the VSD would put excessive stress on the parts, which could damage or potentially destroy the VSD.

2 Variable Speed Drives

Over the past decades, VSDs substantially technologically advanced. They can be classified into three main categories: mechanical, hydraulic and electrical drives. Even though electrical VSDs provide the best speed control, they are more expensive than the mechanical ones, which are still being used. The simplicity of the mechanical drives also contributes to them being favored by many engineers [2], [4].

2.1 Mechanical Variable Speed Drives

As mentioned, mechanical VSDs are still popular due to their simplicity and low cost. The used methods, e.g., belt drives, chain drives, gear boxes, metal friction drives, share similar characteristics, the motor is running at a constant speed, while the output speed of the driven shaft is varied by adjusting the coupling ratio. This type of speed adjustment is very similar to shifting gears on a bicycle. [2] More details on mechanical VSDs can be found in [4].

2.2 Hydraulic Variable Speed Drives

In the hydraulic speed control, the turbine principle is used for hydraulic coupling. The speed on the driven shaft is adjusted by changing the volume of oil present in the coupling. This is achieved by pumps and valves. Another type is fluid coupling [2], [5].

2.3 Electrical Variable Speed Drives

The electrical VSD systems are different from mechanical and hydraulic methods, because they operate the speed of electric motor itself, instead of using the intermediary device. They can either control DC motor, hence they are called *DC drives*, or they can control AC motors, being called *AC drives*. Majority of electrical VSDs are fed from 3-phse AC supply voltage, which mostly consists of pumps, compressors, fans, extruders conveyor belts and others. Historically, best known VSDs were Schrage motor for AC motor and Ward-Leonard system for DC motor [2], [4].

3 Converters

Generally, converters transform specific type of input power into another type of output power. They are categorized into 4 groups – DC-DC converters (Choppers), DC-AC converters (Inverters), AC-AC converters and AC-DC converters (Rectifiers) [6]. The main objective of inverter is to convert DC supply power into an AC output waveform. This type of waveform is used for VSD application and could be divided into two subcategories – direct and indirect. The main difference between them is that the indirect type uses a DC control section, also called DC-link or DC bus [6], [7].

3.1.1 Direct Converters

An example of direct inverters are Cycloconverters and Matrix converters. Cycloconverters use AC power of specific frequency and voltage and convert it to different frequency and voltage. To maintain an allowable waveform and power efficiency the output frequency must be limited to approximately 40% of the input frequency. Despite this, the cycloconverters are still being used for mills and conveyors [8]. E. g., Siemens manufactures cycloconverters up to 4 kV output voltage and 40 MVA of power [9].

Another example of direct inverter is a Matrix converter. These converters are relatively new. The main advantages are 4-quadrant operation, minimal storage requirements and sinusoidal output waveform with minimal higher order harmonics. Its disadvantages are maximum input-output voltage transfer ratio limited to approximately 87% for sinusoidal waveforms, and the demand of more semiconductor devices, compared to indirect converters [10], [11].

3.1.2 Indirect Converters

As mentioned before, the indirect inverters have a DC-link between AC power input and AC power output. They can be further divided into Current source inverters with a current DC-link, and Voltage source inverters with voltage DC-link. For VSDs, more interesting are voltage source inverters. [6]

3.1.3 Two-level Converters

The simplest type of an inverter is a bridge converter also known as a Two-level inverter. A scheme of a three-phase inverter is in Fig. 1. This inverter consists of 2 switches in each phase, that connect the phase either to the positive DC level (+V_{DC}) or negative DC level (-V_{DC}). Connection to the positive level is realized by switching on of the switches in the upper half of the inverter. Connection to the negative level is then done similarly, except the switches in the lower part are being switched on. It is necessary to ensure, that only one switch in each phase is switched on, otherwise the DC-link would be short-circuited, which would damage the devices [6], [12].

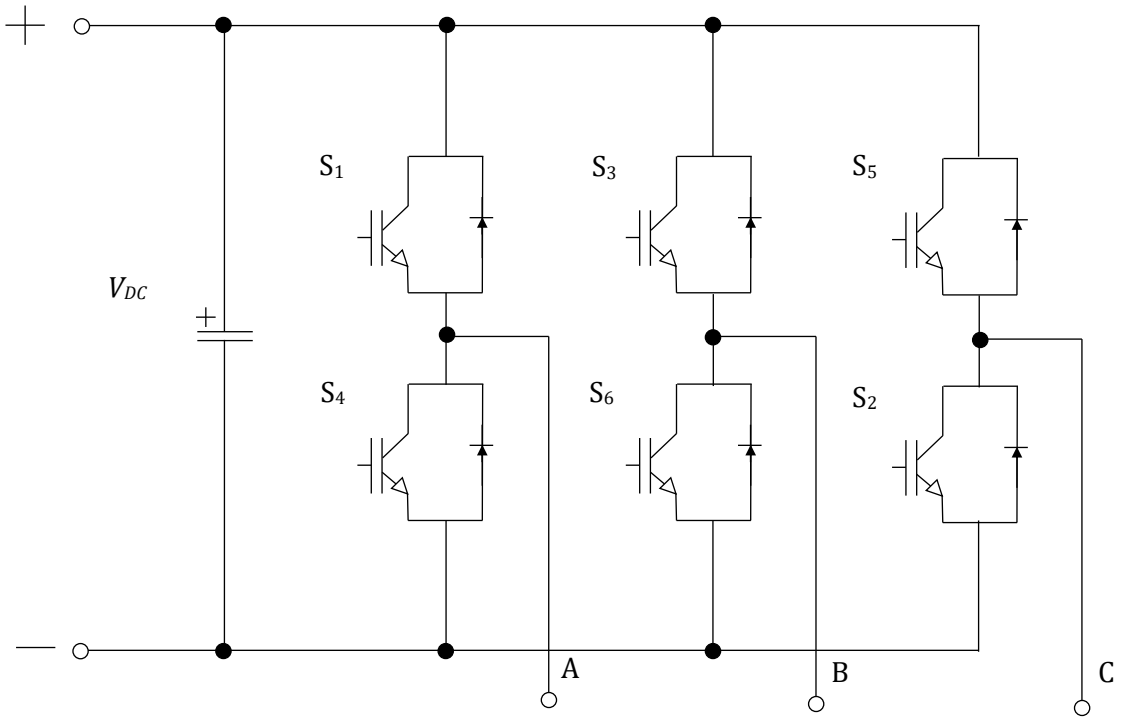

Fig. 1 three-phase two-level inverter

3.1.4 Multilevel Converters

As the name suggests, multilevel converters (MCs) utilize three and more voltage levels between the neutral point and the output leg voltage. The general idea is to divide two bordering levels – upper and lower, into several inner levels. Each level has an equal voltage distance from the neighboring levels. This is done to ensure approximately the same voltages across each device. Control of correct and constant voltage levels is called voltage balancing [6]. As more levels are utilized, the constructed output waveform better resembles the sinusoidal wave with minimum harmonic distortion [13].

There are four major categories for MCs. Cascaded H-bridge topology is said to be the first one, originally introduced in 1975 by Baker and Bannister [6]. Following the invention of cascaded MC, neutral point clamped converter (NPC) was presented in the early 1980's. A decade later, flying capacitor converter was proposed. Last topology is modular multilevel converter (MMC or M^2C) [6]. Switches used in these topologies are mostly transistors such as IGBTs or IGCTs, but there are also converters using SiC MOSFETs. IGBTs and IGCTs are less expensive, compared to MOSFETs, but they have worse thermal properties.

3.1.5 Cascaded H-bridge Topology

Cascaded MC is composed of one-phase converters connected in series, typically called H-bridges. Each bridge consists of n separate DC voltage source, 4 switches and 4 free wheel diodes. The voltage sources must not have the same voltage. If all the DC voltages are same the converter can produce $2n + 1$ output voltage levels and is called symmetrical H-bridge converter. If the source voltages differ, the converter produces $2^{n+1} - 1$ output levels. This type is called asymmetrical H-bridge converter. Asymmetrical topology has the benefit that it can generate more voltage levels with the same amount of voltage sources, compared to the symmetrical topology. However, this causes unequal voltage stress and loss on each device [14].

A 3-phase 5-level cascaded H-bridge is shown in Fig. 2. By switching on switches S_1 and S_4 an output voltage of -V_{DC} can be obtained in the bridge. If switches S_2 and S_3 are turned on, +V_{DC} voltage is on the bridge's output. By turning on combination of either switches S_1 and S_2 or S_3 and S_4, the source voltage is not contributing to the total voltage of one leg [6]. The phase voltage is then result of all bridges summed up together.

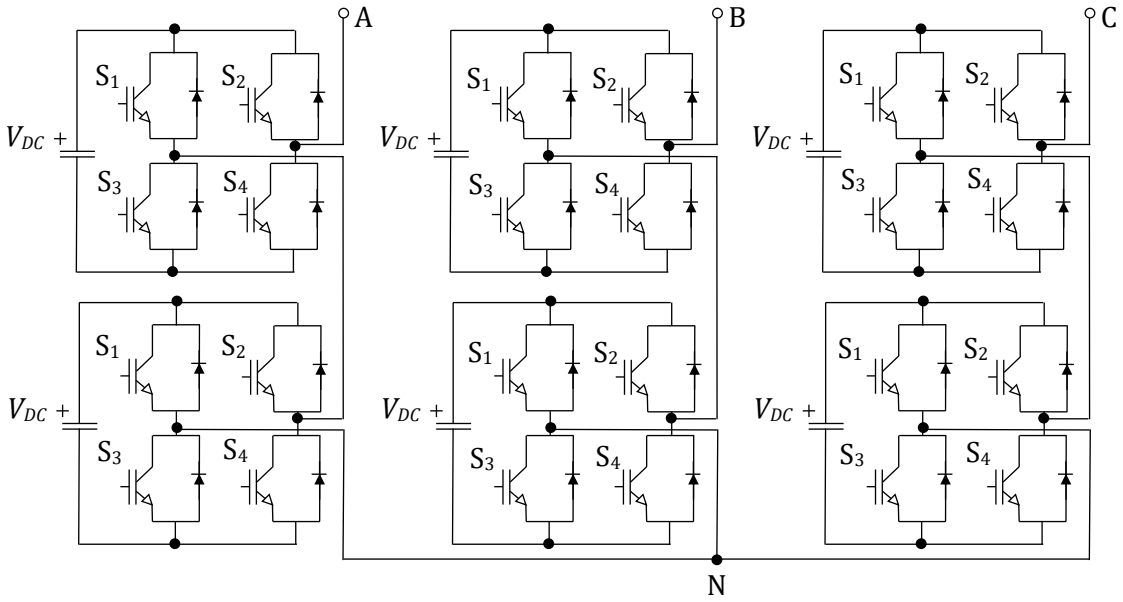

Fig. 2 Symmetrical three-phase five-level cascaded H-bridge

3.1.6 Neutral Point Clamped Topology

In 1980, soon after the introduction of a cascaded H-bridge converter, R. H. Baker presented a new topology, which is a neutral point clamped (NPC) converter. This topology was later improved by Nabae, Takahashi and Akagi with use of just one DC source [6]. NPC converter, also called Diode-clamped multilevel inverter, requires $n - 1$ capacitors to produce n levels of output voltage.

Scheme of a 3-phase 3-level NPC converter is shown in Fig. 3. Each phase of the depicted converter has four switches and two diodes. These two diodes clamp the switch voltage to either $+V_{DC}/2$ or $-V_{DC}/2$, which is half of the voltage of the DC-link. Switches S_{1X}, S_{3X} and S_{2X}, S_{4X} are complementary switching pairs. This means that only one of the switches can be turned on, while the other one remains turned off. If the switches S_{1U} and S_{2U} are turned on, the maximum positive output phase voltage ($+V_{DC}/2$) is obtained. Turning on switches S_{2U} and S_{3U} gives a zero-output phase voltage. The negative output phase voltage ($-V_{DC}/2$) is achieved by turning the switches S_{3U} and S_{4U} on.

Major disadvantages of this topology are that the clamping diodes must have higher voltage ratings for reverse voltage blocking, compared to the ratings of the switches. While increasing the levels of a converter, this becomes more evident. Another downside is that the outer switches (S_{1U}, S_{4U}) conduct only while getting the positive, or negative output voltage, while the inner switches conduct also for zero-output voltage. This unequal conduction duty results in different current rating for switches. Furthermore, it produces different losses between the devices. In [15] it is shown, that using an Active-NPC (ANPC) converter, which uses switches instead of the clamping diodes, can achieve better loss distribution. Finally, by connecting particular output phases to the neutral point, the charging and discharging time for each capacitor is different. Over time, this causes an unbalanced capacitor voltages across different levels [13], [12].

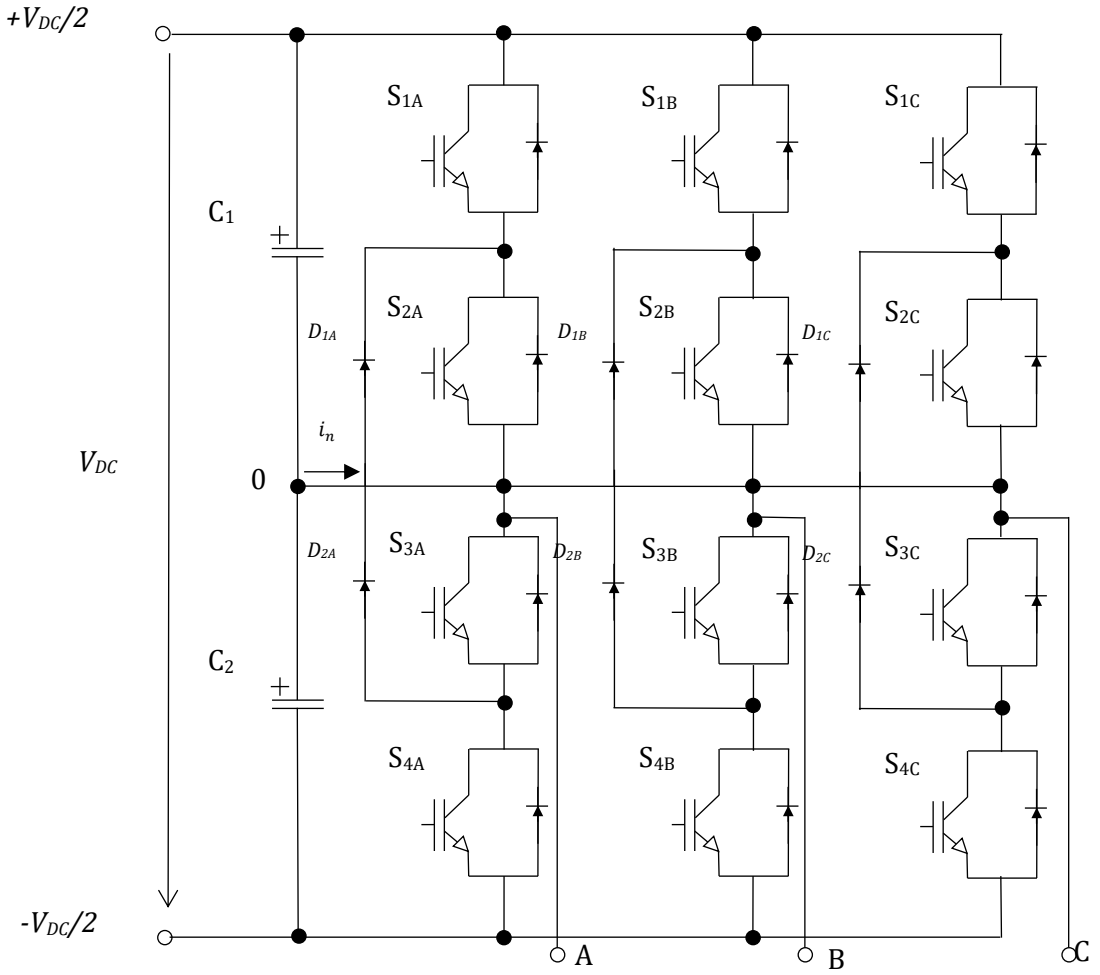

Fig. 3 Three-phase three-level NPC converter

3.1.7 Flying Capacitor Topology

Very similar to the NPC converter is a flying capacitor (FC) converter, presented in 1992 by Meynard and Foch. In this typology, the clamping diode of NPC converter was replaced by a capacitor. The name is derived from the apparent floating of the capacitors with respect to the earth's potential [6].

Three-level FC converter usually uses one flying capacitor for each phase and five-level usually two flying capacitors. In schemes with multilevel FC converters, more flying capacitors are connected in series to indicate the voltage levels between the clamping points, whilst assuming that all these capacitors have the same voltage rating [13]. Three-level three-phase FC converter is shown in a figure below.

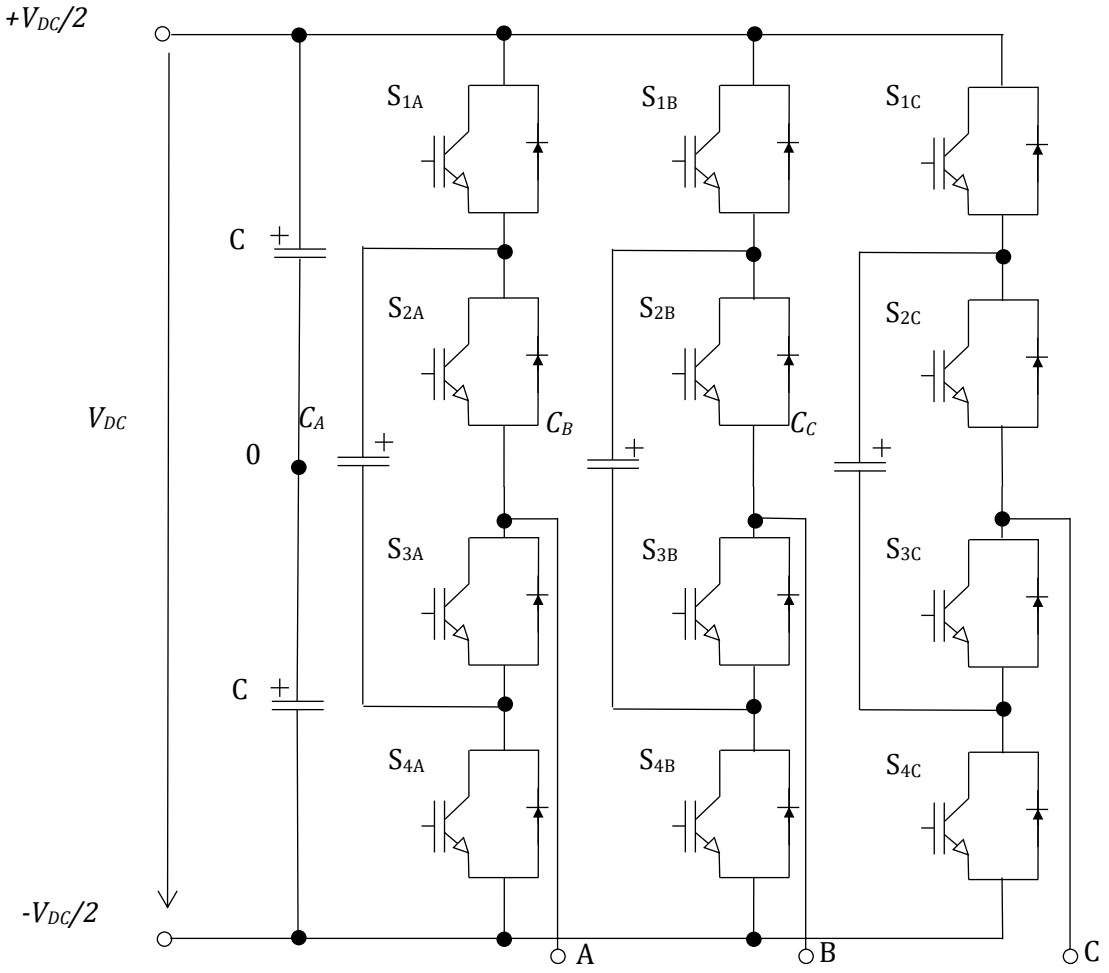

Fig. 4 Three -phase three-level flying capacitor inverter

Using capacitors decreases the amount of needed diodes, thus lowering the drive cost and higher efficiency [12]. During power loss, FC system can still provide power for a limited time. Having a ride-through capability is thanks to the large amount of power stored in many capacitors. This is also a downside of the FC topology, especially when the number of converter levels is high. High-level systems take a lot of space and are more expensive, because of the bulky capacitors [13].

3.1.8 Modular Multilevel Converter Topology

Newest important topology is the modular multilevel converter (MMC or M²C). It was first proposed by Marquardt in 2001. This invention presented a DC to AC converter with series-connected submodules [16]. A basic MMC is made of two arms per phase and each arm consists of N series-connected submodules (SMs) and an inductor connected in series. The inductor is supposed to suppress high-frequency components in the arm current. Each submodule should be nominally identical.

There are various topologies for SMs, the most used are a half-bridge SM and a full-bridge SM. Such a MMC is very similar to the cascaded H-bridge converter. Other less used topologies are the clamp-double circuit, or an SM comprised of previously mentioned NPC or FC topology. These SMs have more voltage levels, but higher losses compared to the half-bridge or even full-bridge submodules. It is also worth mentioning, that the MMC does not need a capacitor in the DC-link, thus decreasing a possibility of its short circuit [6], [17]. A three-phase MMC is presented in Fig. 5.

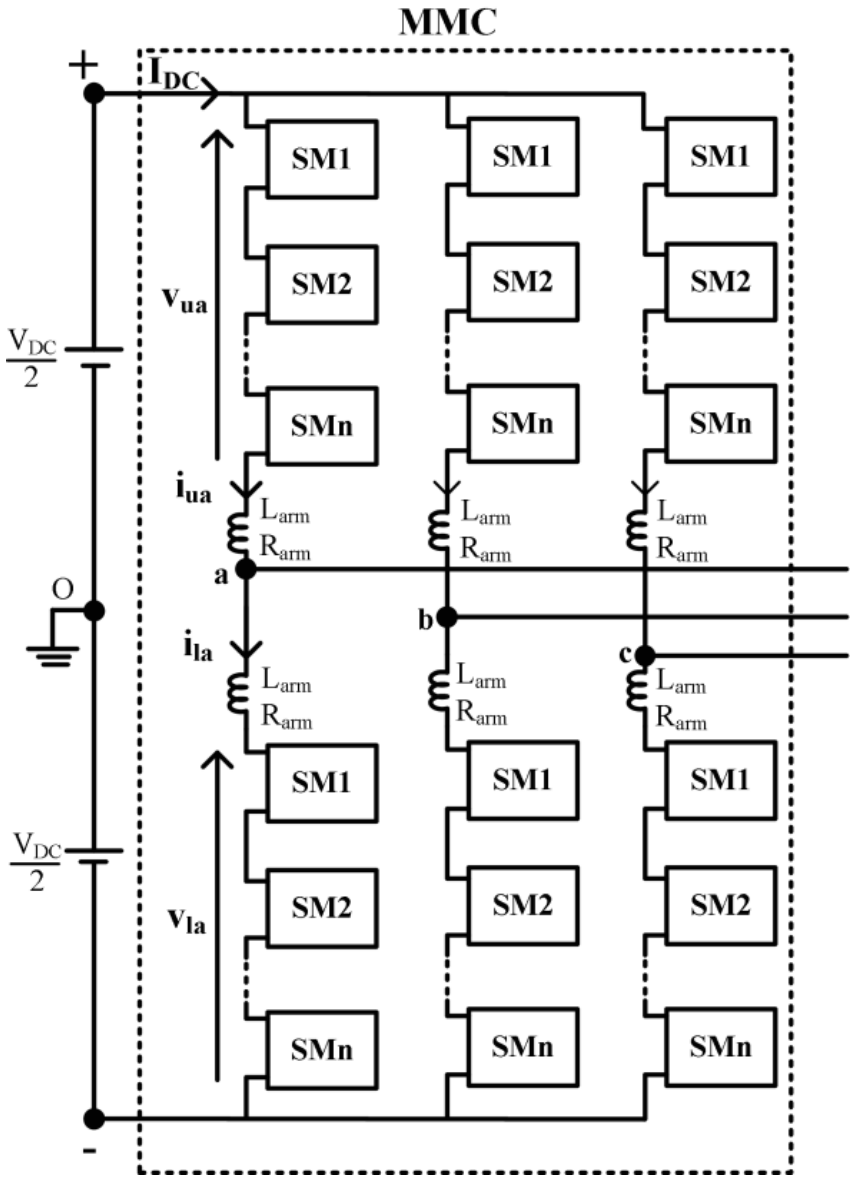

Fig. 5 Three-phase MMC with N series-connected SMs [18]

With the growth of the interest in multilevel converters, many manufactures seized an opportunity and started producing MCs that are either for general use, or specifically designed to fit the needs of their customers. For example, SIEMENS offers wide range of converters cooled by air or water medium. The output voltage ranges from 2.3 kV to 13.8 kV and output power of 4 MVA up to 47.6 MVA for MMC type topology and 1 MVA up to 31.5 MVA for NPC topology. They can be operated as either two-quadrant or four-quadrant systems, using vector control for IGBT, eventually IGCT switches [9].

ABB offers converters with same output voltage as SIEMENS with scalar control or direct torque control (DTC). It is possible to power more motors simultaneously.

Rockwell Automation manufactures converters up to 11 kV in a cascaded H-bridge topology and two quadrant operation. The drives are controlled by either flux vector or V/f scalar control. Switches can be IGBT or SGCT. [19] [20]

Toshiba has in their portfolio three-, five- and seven-level converters with output voltage up to 6.9 kV with the NPC topology. Scalar V/f and sensorless or closed-loop vector controls are implemented in the drives. [21]

TMEIC (Toshiba Mitsubishi-Electric Industrial Systems Corporation) makes similar converters up to 11 kV, with IGBT and IEGT switches. [22]

4 Induction Motor

The most widespread type of motor for electric drives is the induction motor (IM). Its vast use is primarily by their simple construction, which enables manufacturers to build them in mass production. This helps decrease the costs and further supports its spread of use. The simplicity of induction motors affects their control abilities and reliability. Due to the fact, that induction motors can be powered from low voltage household electricity, e. g., small motors in house appliances, and from higher voltages provided by dependent voltage sources, induction motors have very wide spread of utilization [23].

Induction motors can be split into different categories. Usually, they are divided by their output power, size, supply voltage and operation use. They can be further divided by the number of phases, number of poles, rotor construction design, type of protection ad isolation, speed of rotation, etc.

There are three classes if we divide motors by their supply voltage – low voltage, medium voltage and high voltage motors. For the use of multilevel inverters, the medium voltage and high voltage are the most interesting, thus motors with supply voltage over 1000 V. The main advantage of using the higher voltage motors lies in the fact, that considering the same output power, it is possible to use cables for lower electric currents, which is useful for long-distance power transfer over cables and overall costs. These types of motors are usually in a three-phase connection with 2 – 24 poles. It is also possible to get any other number of poles, which are mostly operated as low speed motors. This can be deducted from the equation for the speed of rotating magnetic field:

$$\omega_s = \frac{2\pi \cdot f}{p_p}\ (rad/s) \text{ or } n_s = \frac{60 \cdot f}{p_p}\ (rev/min) \tag{4-1}$$

where ω_s is the synchronous speed in rad/s, f is the supply frequency, p_p is the number of pole pairs and n_s is the synchronous speed in rpm.

Because of the advantages VSDs can provide, there is reasonable offer of motors capable of utilizing a VSD. For example, WEG Industries from Brazil manufactures 3-phase squirrel

cage IM with supply voltage up to 13.8 kV and output power up to 16,000 kW. Number of poles range from 2 to 16. These motors can be run on either 50 Hz or 60 Hz frequency grid and have a protection class IP 65.

SIMOTICS HV line of asynchronous motors, which is produced by Siemens, offers IMs with voltage ranging up to 13.8 kV and output power up to 70 MW. Number of poles spans from 2 to 16 for the highest power motors. Protection class can be as high as IP66 with higher Gas group and Dust group protection.

Slovakian company VYBO Electric manufactures squirrel cage motors with voltages up to 13.8 kV, output of 30 MW. The motors can be manufactured with range of up to 40 poles. It is also possible to get motor with protection class IP 67.

ABB offers squirrel cage IMs with supply voltage ranging from 3 kV to 10 kV and number of poles ranging from 2 to 12 for 50 Hz frequency power grid. At 60 Hz, they offer motors with voltage up to 6.6 kV. For slip ring IMs the voltage can be as high as 11 kV at 50 Hz.

Toshiba has only a few medium voltage motors suitable for VSD. These motors have 4, 6 or 8 poles and work with voltage of 2,300 V or 4,000 V at both 50 Hz and 60 Hz frequency.

4.1 Mathematical Model of the Induction Motor

Induction motor can be transformed from a three-phase balanced system into a two-axis general system (equations (4-2) – (4-5)). This system can be later specified by choosing a reference frame. Although, the speed of rotation ω_c can be arbitrary, there are three main reference frames:

- Stationary reference frame
- Synchronously rotating reference frame
- Rotor reference frame

Sometimes, these reference frames are together called just as a d-q frame, with reference to either stator, rotor, or magnetic field. The presented system of equations uses subscript s, r to indicate either stator or rotor quantities [6] [24] [25] [26]:

$$\bar{V}_s = R_s\bar{I}_s + \frac{d\bar{\Psi}_s}{dt} + j\omega_c\bar{\Psi}_s \tag{4-2}$$

$$\bar{V}_r = R_r\bar{I}_r + \frac{d\bar{\Psi}_r}{dt} + j(\omega_c - \omega_r)\bar{\Psi}_r \tag{4-3}$$

The stator magnetic flux and rotor flux are defined as:

$$\bar{\Psi}_s = L_s\bar{I}_s + L_m\bar{I}_r \tag{4-4}$$

$$\bar{\Psi}_r = L_r\bar{I}_r + L_m\bar{I}_s \tag{4-5}$$

4.1.1 Stationary Reference Frame

Stationary reference frame is occasionally called stator-fixed coordinates system or α-β coordinates system. Because the reference frame is not rotating, speed of rotation ω_c is equal

to zero. Equations are usually written with α, β subscripts and if they are split into real and imaginary components, they will look as:

$$v_{s\alpha} = R_s i_{s\alpha} + \frac{d\psi_{s\alpha}}{dt} \tag{4-6}$$

$$v_{s\beta} = R_s i_{s\beta} + \frac{d\psi_{s\beta}}{dt} \tag{4-7}$$

$$v_{r\alpha} = R_r i_{r\alpha} + \frac{d\psi_{r\alpha}}{dt} + \omega_r \psi_{r\beta} \tag{4-8}$$

$$v_{r\beta} = R_r i_{r\beta} + \frac{d\psi_{r\beta}}{dt} - \omega_r \psi_{r\alpha} \tag{4-9}$$

4.1.2 Synchronously Rotating Reference Frame

In this reference frame, the axes rotate at a synchronous speed $\omega_c = \omega_s$, the speed of rotating magnetic field. It is usually used with a d, q subscripts. Equations split into components can be transformed as:

$$v_{sd} = R_s i_{sd} + \frac{d\psi_{sd}}{dt} - \omega_s \psi_{sq} \tag{4-10}$$

$$v_{sq} = R_s i_{sq} + \frac{d\psi_{sq}}{dt} + \omega_s \psi_{sd} \tag{4-11}$$

$$v_{rd} = R_r i_{rd} + \frac{d\psi_{rd}}{dt} - (\omega_s - \omega_r)\psi_{rq} \tag{4-12}$$

$$v_{rq} = R_r i_{rq} + \frac{d\psi_{rq}}{dt} + (\omega_s - \omega_r)\psi_{rd} \tag{4-13}$$

4.1.3 Rotor Reference Frame

If the axes rotate at the speed of rotor, it is called a rotor reference frame, which is used with d_r and q_r subscripts to show rotor reference. Often the subscript k, l is used. For $\omega_c = \omega_r$, the equations would look as follows:

$$v_{sd_r} = R_s i_{sd_r} + \frac{d\psi_{sd_r}}{dt} - \omega_r \psi_{sq_r} \tag{4-14}$$

$$v_{sq_r} = R_s i_{sq_r} + \frac{d\psi_{sq_r}}{dt} + \omega_r \psi_{sd_r} \tag{4-15}$$

$$v_{rd_r} = R_r i_{rd_r} + \frac{d\psi_{rd_r}}{dt} \tag{4-16}$$

$$v_{rq_r} = R_r i_{rq_r} + \frac{d\psi_{rq_r}}{dt} \tag{4-17}$$

4.1.4 Simulation of Mathematical Model of the Induction Motor

For the simulation purposes, stationary and synchronously rotating reference frames are usually preferred. If the equations for induction motor ((4-2), (4-3)), together with equations for magnetic flux ((4-4), (4-5) are transformed to express stator and rotor currents and then put into stationary reference frame, the squirrel cage induction motor can be simulated using these equations:

$$\frac{di_{s\alpha}}{dt} = \frac{1}{L_s}\left(v_{s\alpha} - R_s i_{s\alpha} - L_m \frac{di_{r\alpha}}{dt}\right) \tag{4-18}$$

$$\frac{di_{s\beta}}{dt} = \frac{1}{L_s}\left(v_{s\beta} - R_s i_{s\beta} - L_m \frac{di_{r\beta}}{dt}\right) \tag{4-19}$$

$$\frac{dir_{\alpha}}{dt} = -\frac{1}{L_r}\left[R_r i_{r\alpha} + L_m \frac{di_{s\alpha}}{dt} + \omega_r\left(L_r i_{r\beta} + L_m i_{s\beta}\right)\right] \tag{4-20}$$

$$\frac{dir_{\beta}}{dt} = -\frac{1}{L_r}\left[R_r i_{r\beta} + L_m \frac{di_{s\beta}}{dt} + \omega_r\left(L_r i_{r\alpha} + L_m i_{s\alpha}\right)\right] \tag{4-21}$$

Together with equations for electromechanical system [26]

$$J\frac{d\omega_m}{dt} = p_p(T_e - T_l) - B\omega_m \tag{4-22}$$

$$T_e = \frac{3}{2}p_p L_m\left(i_{r\alpha} i_{s\beta} - i_{s\alpha} i_{r\beta}\right) \tag{4-23}$$

where J is the moment of inertia of motor and load, ω_m is the mechanical angular speed of the rotor, p_p is the number of pole pairs, T_e is the electromagnetic torque, T_l is the load torque and B is the friction coefficient of the load and motor, model of the induction motor can be developed. This model can be used to simulate and analyze behavior of the motor.

4.1.5 Current Model of the Induction Motor

Also called the I-n model, or I1-n model, this model uses motor's measured supply currents (stator currents) and its rotational speed to determine the rotor magnetic flux, which is used for the motor's control [27] [28] [29]. Using the equation (4-5) for rotor flux and substituting it into equation (4-3) for rotor voltage of a squirrel cage motor

$$0 = \bar{V}_r = R_r \bar{I}_r + \frac{d\bar{\Psi}_r}{dt} + j(\omega_c - \omega_r)\bar{\Psi}_r \tag{4-24}$$

the derivative of rotor flux can be expressed as:

$$\frac{d\bar{\psi}_r}{dt} = \frac{L_m R_r}{L_r}\bar{\imath}_s - \frac{R_r}{L_r}\bar{\psi}_r - j(\omega_c - \omega_r)\bar{\psi}_r \tag{4-25}$$

Choosing a stationary reference frame, where $\omega_c = 0$, equations can be further split into components:

$$\frac{d\psi_{r\alpha}}{dt} = \frac{L_m R_r}{L_r} i_{s\alpha} - \frac{R_r}{L_r}\psi_{r\alpha} - \omega_r \psi_{r\beta} \tag{4-26}$$

$$\frac{d\psi_{r\beta}}{dt} = \frac{L_m R_r}{L_r} i_{s\beta} - \frac{R_r}{L_r}\psi_{r\beta} + \omega_r \psi_{r\alpha} \tag{4-27}$$

If the synchronously rotating reference system is chosen and the d axis of rotating reference frame is aligned with the rotor flux, then $\omega_c = \omega_s$ and the equations system looks as follows:

$$\frac{d\psi_{rd}}{dt} = \frac{L_m R_r}{L_r} i_{sd} - \frac{R_r}{L_r}\psi_{rd} \tag{4-28}$$

$$\omega_{sl}\psi_{rd} = \frac{L_m R_r}{L_r} i_{sq} \tag{4-29}$$

where ω_{sl} is the angular slip speed.

4.2 Control Strategies of the Induction Motor

The control methods for induction motors are usually divided into two categories:

- Scalar control
- Vector control

Some authors may use more categories, such as [30], adding Speed sensorless control and Intelligent control. The speed of squirrel cage IMs can be changed either by changing the number of pole pairs, varying the magnitude of supplied voltage, changing the frequency of the supplied voltage. Changing the number of pole pairs is inefficient and is not widely used anymore. Varying both frequency and voltage is far better solution, because of it simplicity and easy implementation [31].

4.2.1 Scalar control

Scalar control is achieved by the magnitude variation of the control variables. It is sometimes called V/f or V/Hz control, because the voltage to frequency ratio is kept constant. The voltage can be regulated to control the flux and frequency to control torque. However, this disregards the coupling effect in the machine, because flux is also a function of frequency and torque is also a function of voltage. This decreases the dynamic response and makes the system prone to instability. This method is further divided into an Open-loop control and Closed-loop control [31] [30]. In the low speed region, the constant ratio is not applicable, due to the voltage drop over the stator resistance. To keep the original value of the breakdown torque, the voltage drop must be compensated by slower decline of the stator voltage than the decline of the frequency. This is usually done by limiting the bottom limit of the V/f ratio [23].

The open-loop V/f control does not have feedback signal from the motor. Thus, making this method low-cost, simple and immune to feedback error signals. The drawbacks are that the method does not control the torque of the motor. If the load torque is changed, the speed of the motor will change with it [31]. Although this method does not have feedback to control the motor, it is usually accompanied with a stator current sensor to avoid overloads.

The closed-loop V/f control is more precise, compared to the open-loop control. It also controls the torque of the motor. It can be implemented as a speed-control method, in which the desired speed is compared to the actual speed of the rotor and the difference is brought to zero by the PI controller. The closed-loop also contains a slip-control loop, because the slip is proportional to the torque. Another technique is a current-control method, which compares

the desired stator current with the current feedback and is then fed into the PI controller. This method solves the problem of uncontrolled magnetic flux of the speed-control method [23] [31].

4.2.2 Vector control

Vector control uses rotating vectors to control the induction motor. Vector control is sometimes called as Field oriented control (FOC), although FOC is just a subcategory of vector control. Vector control is based on simplification of IM control equations to resemble the equations for separately excited DC motors.

The field oriented control principle is in decoupling the field components into two single-controlled currents – the flux producing current and the torque producing current. This enables the control of flux and torque independently of each other. FOC is achieved by using the reference frames transformations, mentioned in chapter 4.1. To achieve rotor flux orientation, it is necessary to align the rotor flux with the d-axis of the d, q system. Then the q-axis directional component controls the torque [31]. FOC can be further divided depending on the sensors, which are used for feedback signals. The flux and the torque can be either measured or estimated.

Another vector control method is Direct torque control (DTC). This method controls directly torque and magnetic flux of the motor, which means that the measured signals determine directly the state of the switches. Instead of using the d, q synchronous reference frame and orienting on rotor flux as in FOC, direct torque control uses α, β stationary reference frame. Thus, making it more simple and easier to implement. The flux and torque errors are used in the bang-bang controllers (hysteresis controllers). Therefore, it operates in a hysteresis band utilizing a switching table consisting of different voltage vectors and does not involve SVM. This is also its disadvantage, since a reduced number of voltage vectors may cause ripple on the torque [32] [33]. This method can be further improved by using PWM method. With PWM strategy, the high-quality switching patterns result in low-ripple currents and smooth torque and flux waveforms [33].

5 Modulation

Modulation is a process in which parameters of a carrier wave are changed by the reference signal. It is used everywhere, where the information cannot be transferred by carrier signal (wave), especially in electronics and telecommunications. There are 2 important parameters – modulation index and frequency ratio [34].

Modulation index for PWM is defined as ratio between modulated signal and non-modulated signal. High modulation index means that the modulated signal can resemble the reference signal more precisely [34]. However, if the index exceeds 1, the output signal is overmodulated, which leads to clipping of reference signal to the amplitude of carrier wave and introduction of harmonics [35]. This can be utilized when dealing with three-phase inverter, by injecting the third harmonic in the reference signal, thus increasing the ratio to $2/\sqrt{3} \cong 1.155$ [6].

PWM usually presents modulation index as a ratio of amplitude of the reference signal A_r and amplitude of the carrier wave A_c:

$$M = \frac{A_r}{A_c} \tag{5-1}$$

Second parameter, the frequency ratio, is defined as ratio of the carrier wave frequency f_c to the reference signal frequency f_r. Higher ratio means that the output voltage contains more of fundamental frequency [34].

$$P = \frac{f_c}{f_r} \tag{5-2}$$

5.1 Modulation of Multilevel Converters

Among all modulation techniques, the pulse width modulation is the most popular and widely used by MLC manufacturers. Unlike square wave inverter, which can control only the frequency of output voltage, PWM can control the frequency, amplitude and harmonics included in the output voltage [36]. Modulations can be compared by several attributes, such as harmonic generation, switching losses, response speed or distortion of modulated signal. Classification of PWM techniques is not unified and one method can have multiple names. Nevertheless, there are three main categories [6]:

- Programmed PWM
- Carrier-based PWM
- Space vector PWM

5.2 Programmed Pulse Width Modulation

This technique uses offline precalculated PWM switching pattern, which stores in memory for later online access. Programmed PWM also optimizes the desired performance criteria, e.g., eliminating low-order harmonics, reducing total harmonics, or minimizing the switching frequency. Therefore, this method is also called optimal PWM. Because of the difficulty to correctly produce switching patterns in the transient state or DC-link voltage deviation, this technique cannot be used for fast dynamic systems [36].

5.3 Carrier-based Pulse Width Modulation

This method is similar to the two-level technique which is explained in [34]. Implementation for N-level converter requires N-1 carrier waves. They usually have sawtooth or triangle shape and are symmetrically distributed with respect to the zero axis. All carrier waves have the same frequency and same peak-to-peak amplitude. These carriers are then compared with the reference signal, typically a sine wave, resulting in output modulated signal. From this signal are then created gate pulses for converter switches. This modulation is called Sinusoidal PWM (SPWM), also known as Subharmonic PWM or Suboscillation PWM. There are three basic ways how to mutually dispose the triangle carriers [6]:

- Alternative Phase Opposition Disposition (APOD) – all carriers are in opposition
- Phase Opposition Disposition (POD) – all positive carriers are mutually in phase, but in opposition with the negative ones
- Phase Disposition (PD) – all carriers are in phase

Dispositions are shown in Fig. 6.

With high frequency ratio P, all three modulations have similar qualities. With low P, the PD SPWM underperforms others due to the content of harmonics. This changes in the three-

phase performance, since these harmonics disappear and finally outperforms others with the lowest harmonics distortion [6].

With respect to the N-level converter with N-1 carrier waves, the modulation index from equation (5-1) can be changed to the following form [6]:

$$M = \frac{A_r}{(N-1) \cdot A_c} \tag{5-3}$$

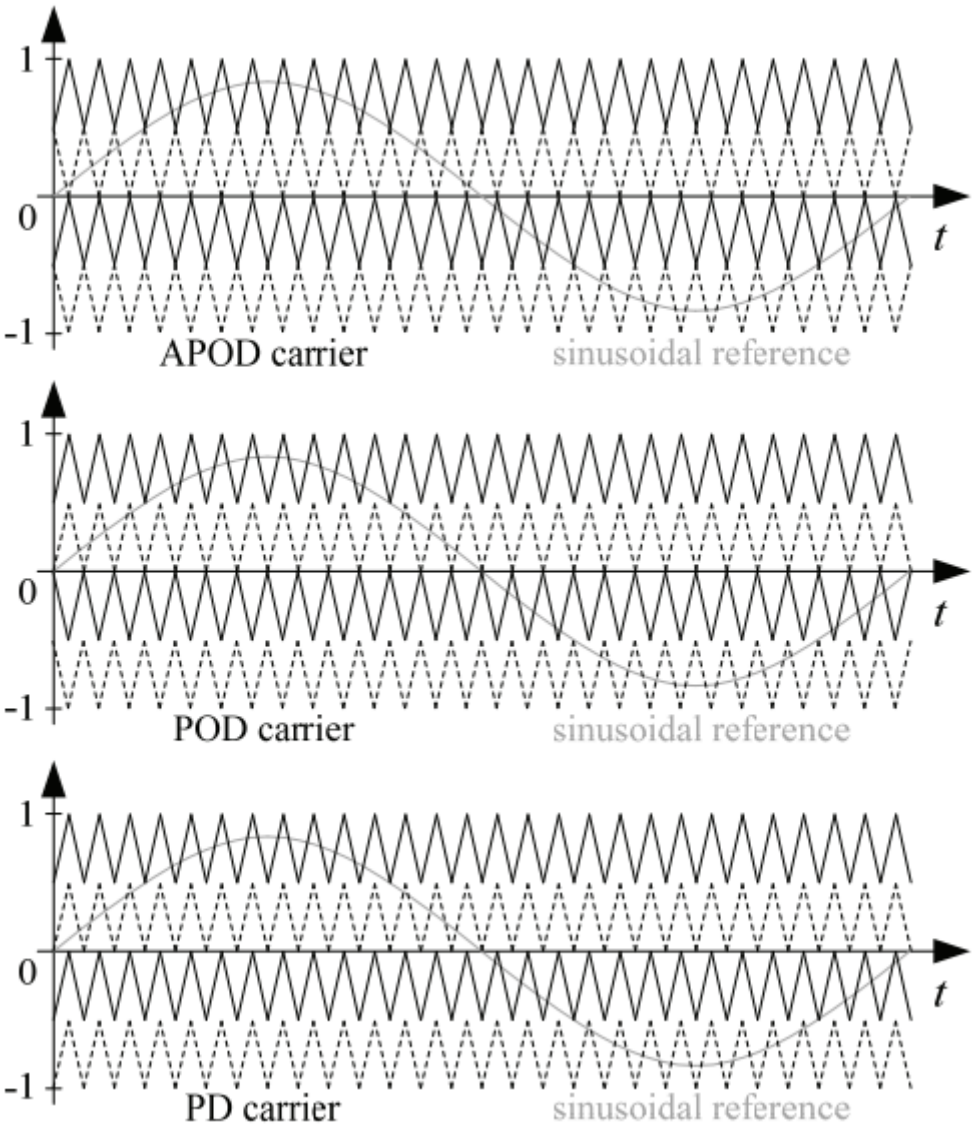

Fig. 6 SPWM dispositions for five-level flying capacitor converter (M = 0.83, P = 28) [6]

5.4 Space Vector Pulse Width Modulation

Space vector PWM (SVPWM), also called Carrierless PWM or simply Space vector modulation, is a method in which the pulses placement is explicitly stated. Each level of output voltage increases the number of possible switching states, making the modulation more complex. The

desired output phase voltages V_a, V_b, V_c are represented by the reference voltage space vector $\bar{V}_{ref}$.

$$\begin{pmatrix} \bar{V}_\alpha \\ \bar{V}_\beta \end{pmatrix} = \frac{2}{3}\begin{pmatrix} 1 & -1/2 & -1/2 \\ 0 & \sqrt{3}/2 & -\sqrt{3}/2 \end{pmatrix}\begin{pmatrix} v_a \\ v_b \\ v_c \end{pmatrix} \tag{5-4}$$

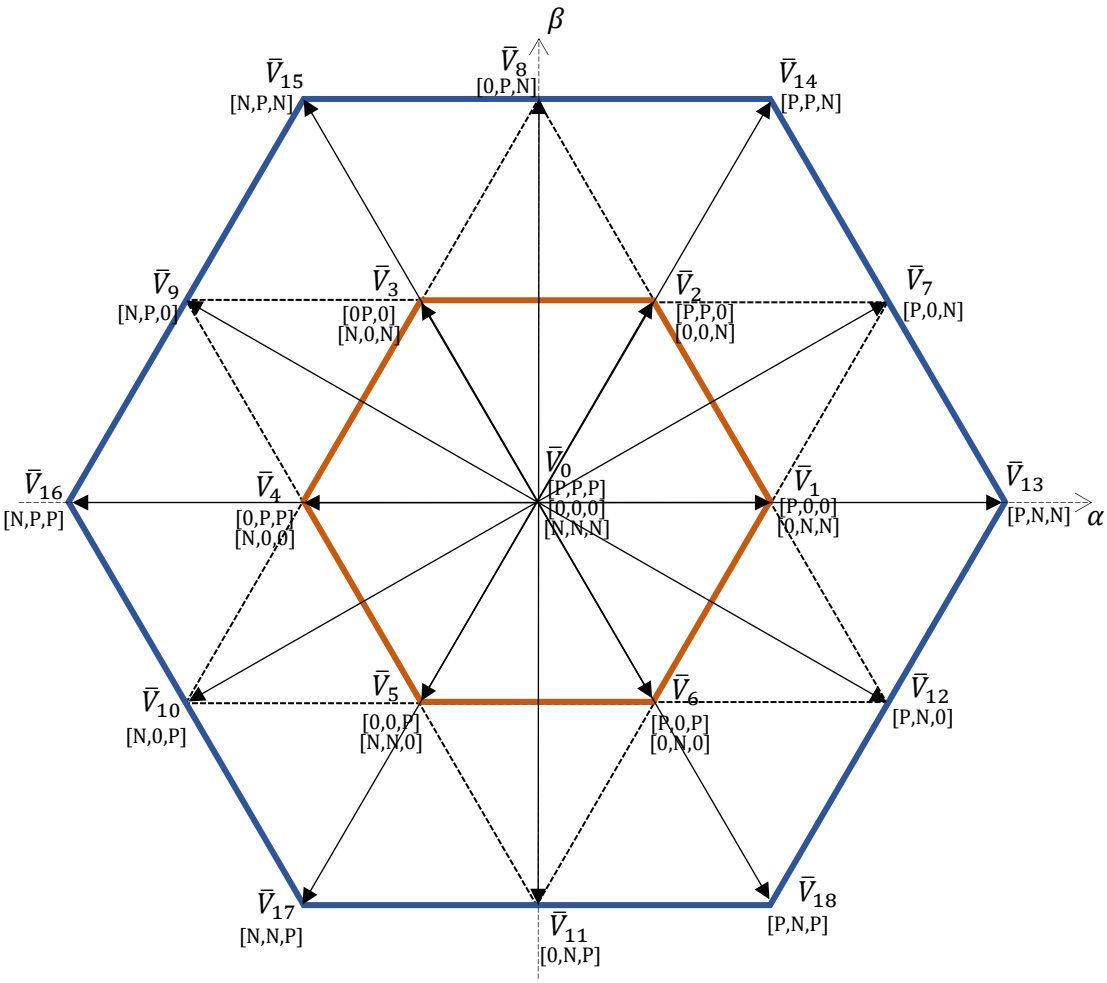

Fig. 7 Space vectors of a three-level converter

For a three-phase three-level converter, the output voltages for each leg are either $+V_{DC}/2$, 0 or $-V_{DC}/2$. By using an α-β transformation for balanced system (equation (5-4)), the phase voltages can be transformed into stationary two-axis reference frame, resulting in space vectors. This leads to 19 space vectors with 27 permissible switching states. These space vectors can be further divided based on their magnitude into [6] [37]:

- Small vectors $\bar{V}_1$ – $\bar{V}_6$ with magnitude of $V_{DC}/3$
- Medium vectors $\bar{V}_7$ – $\bar{V}_{12}$ with magnitude of $V_{DC}/\sqrt{3}$
- Large vectors $\bar{V}_{13}$ – $\bar{V}_{18}$with magnitude of $2V_{DC}/3$
- Zero voltage vector $\bar{V}_0$ with zero magnitude

Medium and large vectors can be achieved by exactly one switching combination. Zero vector can be switched by three possible combinations and small vectors have two switching states, which can be further divided into P-type or N-type vectors. P- and N-type vectors are utilized for voltage balancing of capacitors in the DC-link. Putting the vectors into a complex plane and connecting nearest three vectors, two hexagons divided into smaller triangles emerge. Every additional level then adds hexagon and triangles to the plane [37].

SVPWM defines the modulation index as [34]:

$$M = \frac{\sqrt{3}\bar{V}_{ref}}{V_{DC}} \tag{5-5}$$

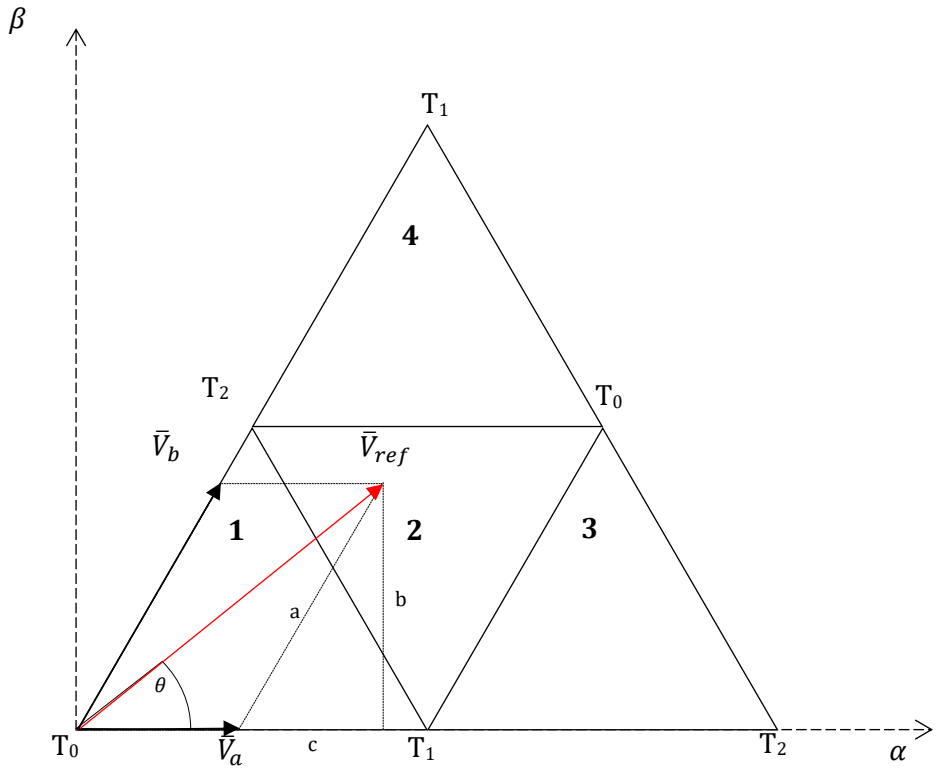

Fig. 8 Space vector diagram of sector 1

5.4.1 Nearest Three Vector Modulation

As the name suggests, this method uses three nearest vectors surrounding the reference vector. These small triangles from Fig. 7 represent areas called Regions and together Sectors. There are 6 sectors, each with 4 regions. Because of the circular symmetry, it is sufficient to consider only one sector and apply results to the rest with appropriate rotation. The reference vector is synthetized by the SVM of the nearest three vectors at every sampling instant [38]. Determining in which sector the reference vector lies is not difficult and can be calculated as:

$$\theta = \operatorname{atan}\left(\frac{\bar{V}_\beta}{\bar{V}_\alpha}\right) \tag{5-6}$$

The particular region selection is derived followingly [39]:

$$\bar{V}_b = a = \frac{b}{\sin\frac{\pi}{3}} = \frac{2}{\sqrt{3}}b = \frac{2}{\sqrt{3}} \cdot \bar{V}_{ref} \cdot \sin\theta \tag{5-7}$$

$$\bar{V}_a = \bar{V}_{ref} \cdot \cos\theta - a \cdot \cos\frac{\pi}{3} = \bar{V}_{ref} \cdot \cos\theta - \frac{2}{\sqrt{3}} \cdot \bar{V}_{ref} \cdot \sin\theta \cdot \cos\frac{\pi}{3} = \\ = V_{ref}\left(\cos\theta - \frac{\sin\theta}{\sqrt{3}}\right) \tag{5-8}$$

Region is then selected by the following rules:

1. If $\bar{V}_a, \bar{V}_b$ and $\bar{V}_a + \bar{V}_b$ is less than small vector's magnitude $V_{DC}/3$, $\bar{V}_{ref}$ lies in region 1.
2. If $\bar{V}_a$ and $\bar{V}_b$ are less than $V_{DC}/3$ and $\bar{V}_a + \bar{V}_b$ is greater than $V_{DC}/3$, $\bar{V}_{ref}$ is in region 2.
3. If $\bar{V}_a$ is greater than $V_{DC}/3$, $\bar{V}_{ref}$ is located in region 3.
4. If $\bar{V}_b$ is greater than $V_{DC}/3$, $\bar{V}_{ref}$ is in region 4.

The reference vector presented in Fig. 8 is synthesized as follows:

$$\bar{V}_{ref} = \frac{T_1}{T_s}\bar{V}_1 + \frac{T_2}{T_s}\bar{V}_{13} + \frac{T_0}{T_s}\bar{V}_7 \tag{5-9}$$

$$T_1 + T_2 + T_0 = 1 \tag{5-10}$$

where T_1, T_2, T_0 are dwell times for selected vectors $\bar{V}_1, \bar{V}_{13}, \bar{V}_7$ respectively and T_s is the switching period.

Dwell times can be derived substituting the magnitudes of each vector together with their rotation into equation (5-9) as [40]:

$$V_{ref}e^{j\theta} = \frac{T_1}{T_s}\frac{V_{DC}}{3} + \frac{T_2}{T_s}\frac{2}{3}V_{DC} + \frac{T_0}{T_s}\frac{V_{DC}}{\sqrt{3}} \cdot e^{j\frac{\pi}{6}} \tag{5-11}$$

Applying the Euler's formula

$$V_{ref} \cdot (\cos\theta + i \cdot \sin\theta) \\ = \frac{T_1}{T_s}\frac{V_{DC}}{3} + \frac{T_2}{T_s}\frac{2}{3}V_{DC} + \frac{T_0}{T_s}\frac{V_{DC}}{\sqrt{3}} \cdot \left[\cos\left(\frac{\pi}{6}\right) + i \cdot \sin\left(\frac{\pi}{6}\right)\right] \tag{5-12}$$

Using equations (5-10) and (5-12), the dwell times are following:

$$T_1 = T_s\left(2 - \frac{3V_{ref}}{V_{DC}} \cdot \cos\theta - \frac{\sqrt{3}V_{ref}}{V_{DC}} \cdot \sin\theta\right) \tag{5-13}$$

$$T_2 = T_s\left(-1 + \frac{3V_{ref}}{V_{DC}} \cdot \cos\theta - \frac{\sqrt{3}V_{ref}}{V_{DC}} \cdot \sin\theta\right) \tag{5-14}$$

$$T_0 = T_s\left(\frac{2 \cdot \sqrt{3}V_{ref}}{V_{DC}} \cdot \sin\theta\right) \tag{5-15}$$

Together with equation (5-4) the previous equations can be further simplified:

$$T_1 = T_s\left[2 - M \cdot \left(\sqrt{3}\cos\theta - \sin\theta\right)\right] \tag{5-16}$$

$$T_2 = T_s\left[-1 + M \cdot \left(\sqrt{3}\cos\theta - \sin\theta\right)\right] \tag{5-17}$$

$$T_0 = T_s \cdot 2 \cdot M \cdot \sin\theta \tag{5-18}$$

Combining space vectors with their assigned dwell times results in a switching sequence that can be specifically organized to eliminate or minimize certain unwanted elements. Conventional SVM breaks the total switching period into seven-segment pulse pattern, symmetrically centered around the middle of the sequence. This is done to reduce the switching losses and for better harmonics composition. Dividing the sequence into seven segments also helps with voltage balancing of the capacitors in the DC-link. This is because in regions 3 and 4 are one large, one medium and one small vector. Splitting the small vector (in this case vector $\bar{V}_1$) in two halves and using both P-type and N-type vectors, minimizes the neutral point deviation. However, in regions 1 and 2 are two small vectors with one zero voltage vector or one medium vector, respectively [37]. Effects of switching states on neutral point voltage deviation is presented in Fig. 10.

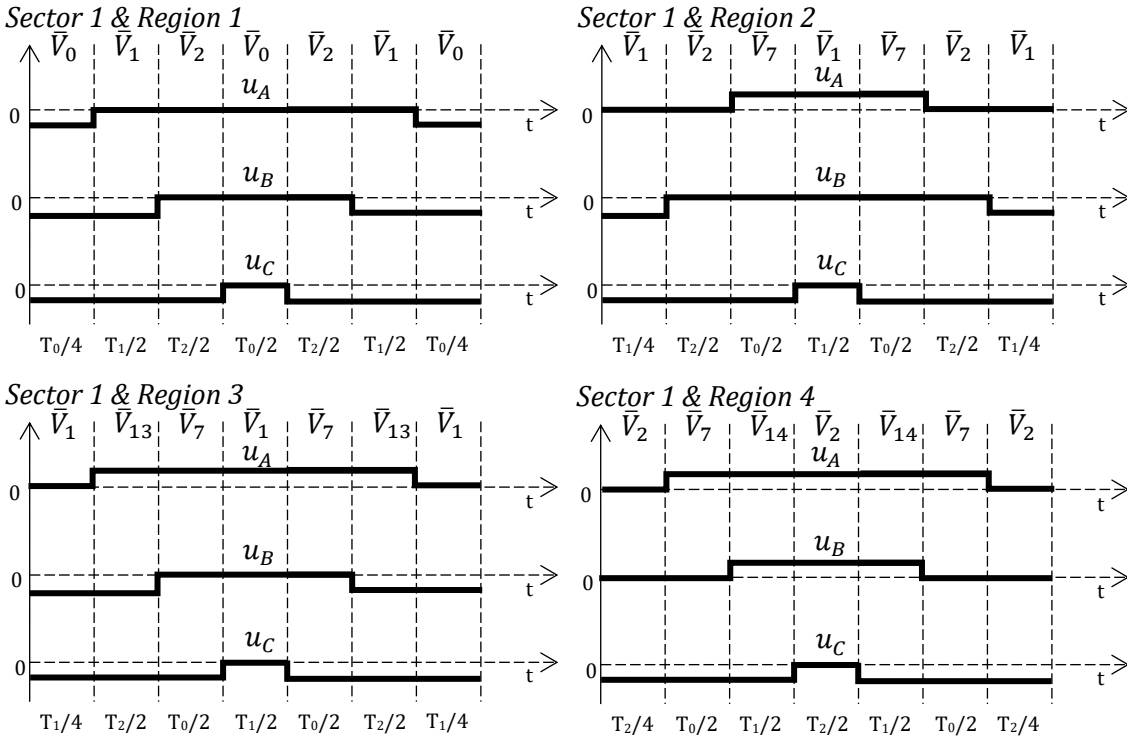

Fig. 9 Negative switching sequences for sector 1

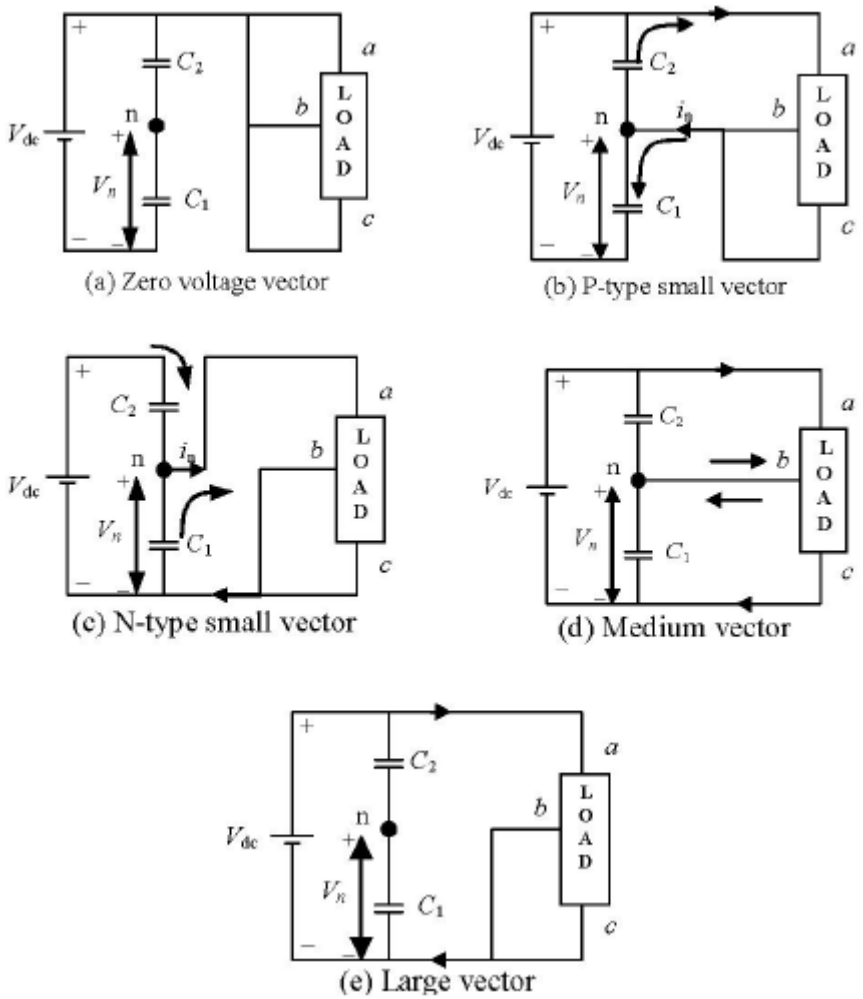

Fig. 10 Effect of switching states on Neutral point voltage deviation [37]

Zero voltage and large vectors have no effect on neutral point voltage, since the neutral point n is not connected to the load. Medium vectors depend on the inverter operating conditions and the neutral point voltage V_n may rise or drop. Small vectors, which are either P-type or N-type have clear effect on the neutral point. P-type vectors cause the neutral current i_n to flow into n, hence increasing the voltage of lower capacitor. N-type vectors have the opposite effect and discharge the lower capacitor [37]. This fact is later used in the simulation to balance the capacitors' voltages.

Switching sequences, as seen in Fig. 9, are for sector 1 and regions 1 – 4. Since there are three possible levels for each leg of the inverter (P, 0, N), which are represented by the space vectors, the duty cycles must be calculated in two levels. These two duty cycles are then added together to create the reference signal. This essentially means calculating the duty cycle as in two-level inverter with SVPWM control, and then shifting it up appropriately, to get additional output level. The tables with positive switching sequences for first sector and all phases are shown below. First table is for the sequencing of dwell times, respectively space vectors. Second table is for the shift.

Table 1 Duty cycle of the positive switching sequence for sector 1

Sector 1	Phase A	Phase B	Phase C
Region 1	$T_1 + T_2 + T_0/2$	$T_2 + T_0/2$	$T_0/2$
Region 2	$T_1 + T_2/2 + T_0$	$T_2/2$	$T_1 + T_2/2$
Region 3	$T_1/2 + T_2 + T_0$	$T_1/2 + T_0$	$T_1/2$
Region 4	$T_1 + T_2/2 + T_0$	$T_1 + T_2/2$	$T_2/2$

Table 2 Duty cycle of the positive shift for sector 1

Sector 1	Phase A	Phase B	Phase C
Region 1	$T_1 + T_2 + T_0$	$T_1 + T_2 + T_0$	$T_1 + T_2 + T_0$
Region 2	$T_1 + T_2 + T_0$	$T_1 + T_2 + T_0$	0
Region 3	$T_1 + T_2 + T_0$	0	0
Region 4	$T_1 + T_2 + T_0$	$T_1 + T_2 + T_0$	0

It can be observed that the shift table has either value of $T_1 + T_2 + T_0$, or 0. All dwell times added together are equal to 1. This is meant by the shift, that moves the switching sequence from the first table up, when the shift is 1, or moves it down, when the shift is 0. The process then follows the one used in SPWM – comparing the reference vector with carrier waves and synthesizing gate signals for electronic switches.

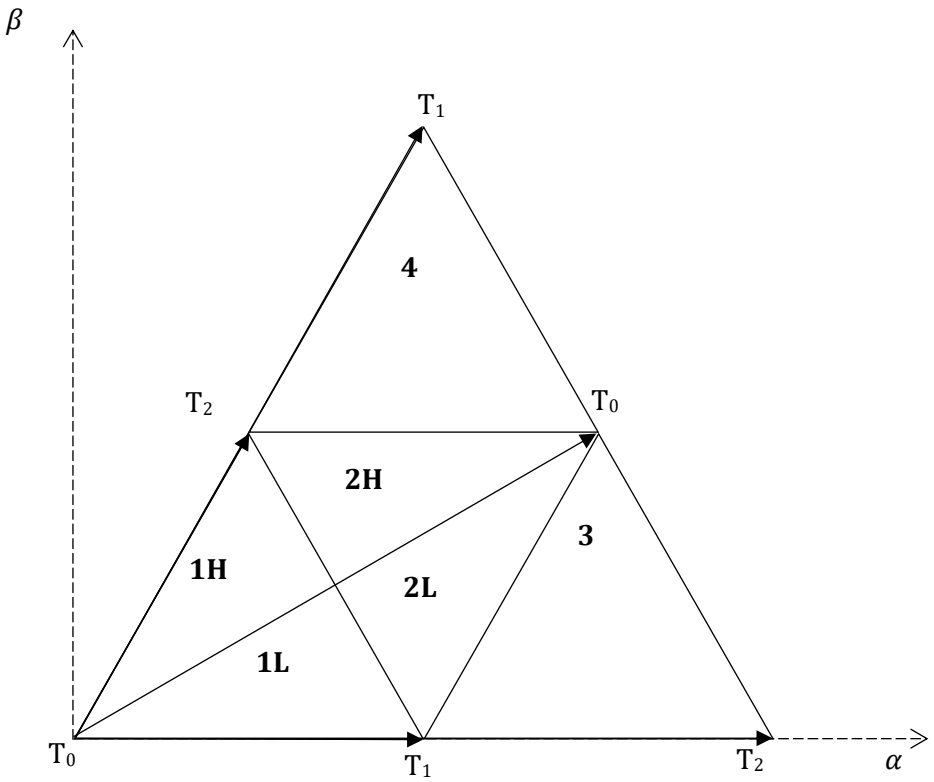

Fig. 11 Region distribution for Symmetric space vector modulation

5.4.2 Symmetric Modulation

Another method used for SVPWM is Symmetric modulation. Although symmetric modulation is sometimes interchanged for symmetrical modulation, which is symmetrically organized switching pattern, this modulation uses four vectors instead of just three. This should theoretically eliminate the neutral point deviation. This is true to some extent, because symmetric modulation produces higher amplitudes of low-frequency oscillations in the voltages of the capacitors [41].

The procedure follows the one for the nearest three vector (NTV) modulation with exceptions in the construction of switching sequence. In regions 3 and 4, the switching sequence looks same for both the NTV modulation using seven-segment pulse pattern, and the symmetrical modulation. The difference is in regions 1 and 2, where each region is split in two, representing P-type vectors and N-type vectors. A variation of this method is later used in the simulation for voltage balancing of the capacitors. Diagram showing the distribution of regions of symmetrical modulation is in Fig. 11.

6 Simulation Model of the Multilevel Converter

Simulation is performed in MATLAB/Simulink interface using Simulink and Simscape library. Simulink library is used for computation and control techniques, while Simscape library allows to model physical network models. Simulink allows easy modification of parameters, which is very useful for the simulation of multilevel converter. The model is divided into parts and subsystems:

- Simscape part
  - Rectifier
  - Neutral point clamped inverter
  - Asynchronous machine
- DC-link pre-charge subsystem
- Control
- SVPWM
- Mathematical model of IM
- Measurements

The Simscape part resembles the VSD's functional structure mentioned in chapter 1, where the grid supply voltage is rectified, then inverted and then finally fed to the induction motor. Control subsystem contains different control methods and outputs the $\alpha\beta$ voltage reference for the SVPWM, where it is modified to give the signals for the NPC converter.

Area "Switch operation" is used to switch between the control methods and area "Requested values" is used to give the reference speed, load torque or value of rotor magnetic flux.

Motor parameters for simulation are in chapter 6.12 and whole code file, that is used mostly for calculation of constants, is in Appendix B. Simulation is carried out using 1 μs fixed-step size and fourth-order ODE with Runge-Kutta method.

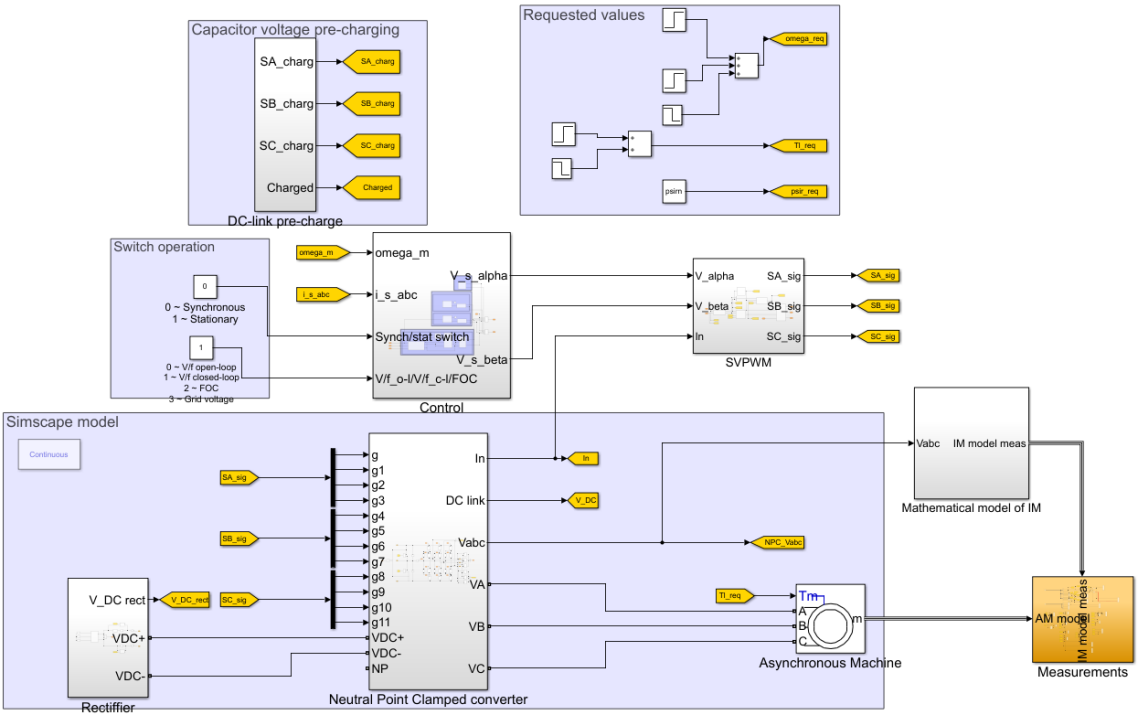

Fig. 12 Simulation model

6.1 Rectifier

Rectifier subsystem consists of grid voltage which is fed directly into the rectifier. Rectified DC voltage is then fed into a charging circuit. The charging circuit is used for pre-charging the capacitors in DC-link and consists of induction and resistor to smooth out the voltage and current spikes . After the capacitors are fully charged, ideal switch flips and bypasses the charging elements. The DC voltage is being measured and can be compared with the DC-link voltage if needed.

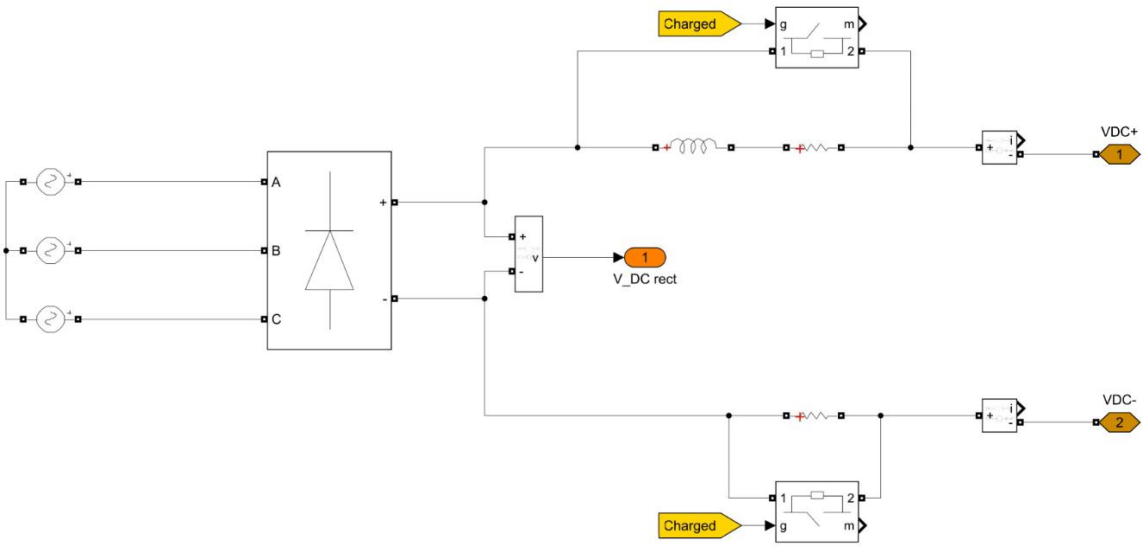

Fig. 13 Rectifier

6.2 DC-link pre-charging

To provide optimal starting point for MMC operation, the capacitors in the DC-link must be fully charged. This is accomplished by comparison of capacitors' voltages and estimated DC-link voltage. There are two blocks "*Approx. equal*" which compare the relative deviation of two inputs. In this case, they compare voltage between both capacitors, and voltage between each capacitor and estimated DC-link voltage. After both capacitors have approximately the same voltage as the DC-link voltage, the "*Charged*" signal is changed to 1, otherwise it stays 0.

From experiments, it is faster to bring the capacitors on equal voltage and then proceed to charge them. This is implemented in the "*Pre-charge boost*" subsystem. Depending on the capacitors' voltage levels, one of them is discharged to match the voltage of the second one, using the neutral point deviation effect depicted in Fig. 10. After, the switches of MMC are turned off, to allow the capacitors to charge.

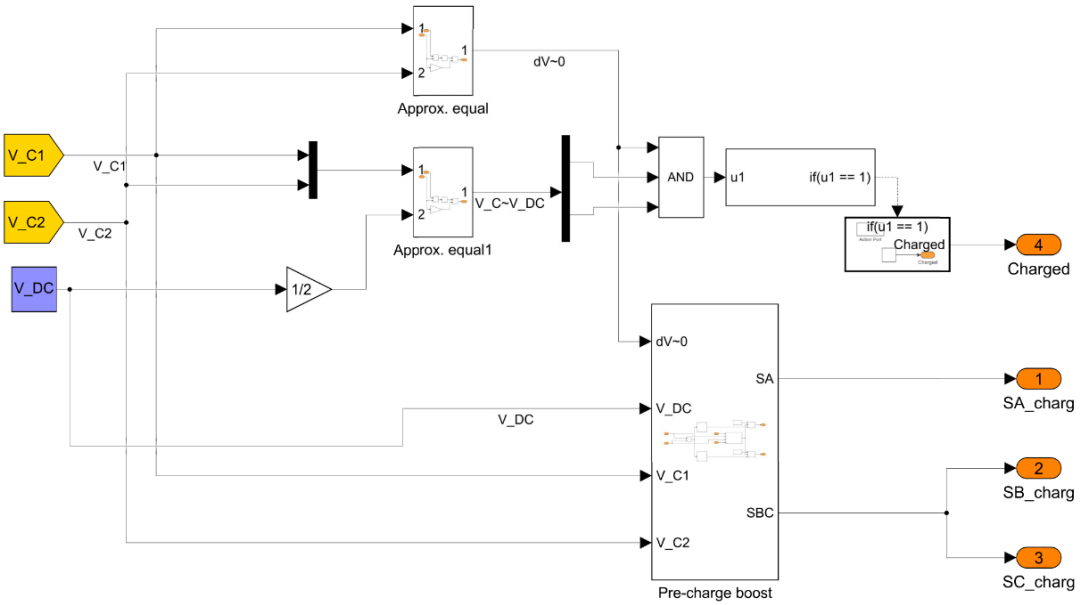

Fig. 14 DC-link pre-charge

6.3 Control

This simulation model has four control methods to achieve the reference quantities. There are two scalar methods, one without feedback and one with mechanical speed feedback. Then there is a vector control using the current model from chapter 4.1.5 with the stationary reference frame and the synchronously rotating reference frame. Output of every type of control is voltage, transformed into $\alpha\beta$ reference frame. To switch between each of the control method a Multiport switch is used that can be controlled from outside of the subsystem.

6.4 V/f Open-Loop Control

Scalar open-loop control consists primarily of a lookup table and reference vector synthetization. The reference speed is converted in lookup table into appropriate frequency according to the $V/f = const.$ ratio. The ratio is limited from 10 % to 100 % of nominal frequency, due to low speed region. The output frequency is then fed into a slew rate limiter

multiplied by a signal from ramp. The ramp signal is to make the limiter start from zero and is restricted to 1. In case there is no reference speed send, the frequency will gradually increase to nominal frequency, due to another implemented ramp. The frequency is then used to synthesize the sinusoidal waveform and the reference vector.

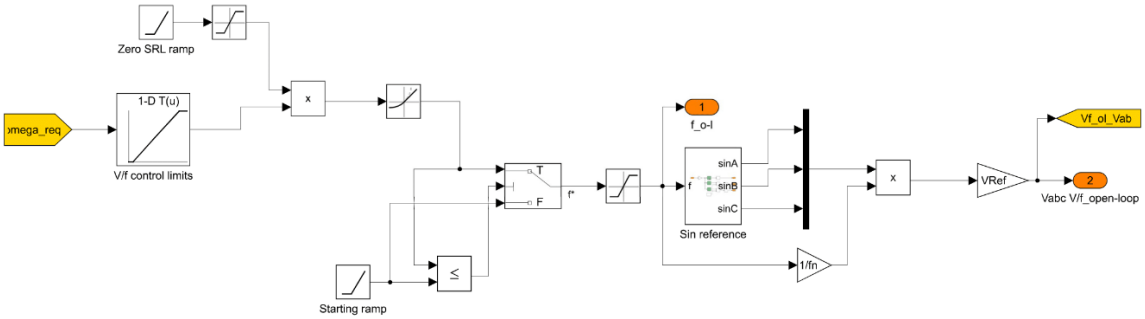

Fig. 15 V/f open-loop

6.5 V/f Closed-Loop Control

Scalar closed-loop control uses the mechanical speed as feedback, which is compared to the reference speed. The error is then fed into PID controller. Resulting slip speed is then added together with the mechanical speed to get the synchronous speed. The synchronous speed is limited by the reference speed and is fed into a rate limiter to be later transformed into frequency. There is also a ramp, similarly to open-loop control, to force the rate limiter to start from zero. The frequency is fed into a lookup table with output between 0 and 1 to appropriately scale the final voltage waveform. The final waveform is synthesized in the "*Sin reference*" block, and appropriately scaled by the output from the lookup table.

6.6 Vector control

Vector control, specifically field oriented control, uses two current models to obtain the rotor flux. These models were built according to equations (4-26) – (4-29). The rotor flux is then compared to the reference value of the flux and the error is fed into a PID controller, giving the desired value of the d-axis component of stator current. The d-axis components are then compared, and the error is fed into another PID controller, which results in the final d-axis component of the stator voltage.

Same procedure is for the q-axis components of stator voltage, except the input to the first controller is not magnetic flux, but mechanical speed. After comparing the desired and actual mechanical speed and feeding the error into a PID controller, i_{sq} is obtained and the process follows the d-axis component mentioned before. Finally, the V_{sq} is acquired.

The dq voltages are then transformed into $\alpha\beta$ reference frame which is used for SVPWM.

Limits for PID controllers were taken from [28] and derived from the equation for stator voltage (4-2). Assuming the steady state of induction motor, the nominal stator flux can be calculated from the induction motor vector diagram as:

$$\psi_{sn} = \frac{\sqrt{(\sqrt{2}V_{ln} - R_s\sqrt{2}I_n\cos\varphi)^2 + \left(R_s\sqrt{2}I_n\sin\varphi\right)^2}}{\omega_{mn}} \tag{6-1}$$

where the subscript n means nominal value.

The nominal dq components of rotor flux and its magnitude are calculated as:

$$\psi_{rdn} = \frac{L_r}{L_m}(\psi_{sdn} - \sigma L_s I_{sdn}) \tag{6-2}$$

$$\psi_{rqn} = \frac{L_r}{L_m}(\psi_{sqn} - \sigma L_s I_{sqn}) \tag{6-3}$$

$$\psi_{rn} = \sqrt{\psi_{rdn}^2 + \psi_{rqn}^2} \tag{6-4}$$

where σ is the leakage factor.

Finally, the dq components of stator current can be expressed as:

$$I_{sdn} = \frac{\psi_{rn}}{L_m} \tag{6-5}$$

$$I_{sqn} = \frac{2L_r M_n}{3p_p L_m \psi_{rn}} \tag{6-6}$$

6.7 Space Vector Modulation

As it was described in chapter 5.4, the space vector modulation is accomplished in parts, represented by the subsystems. At first, the obtained voltage in stationary reference frame is transformed into reference vector using simple trigonometry. Secondly, the sector and region are chosen. Then the dwell times are calculated. And finally, the duty cycles for each leg are calculated.

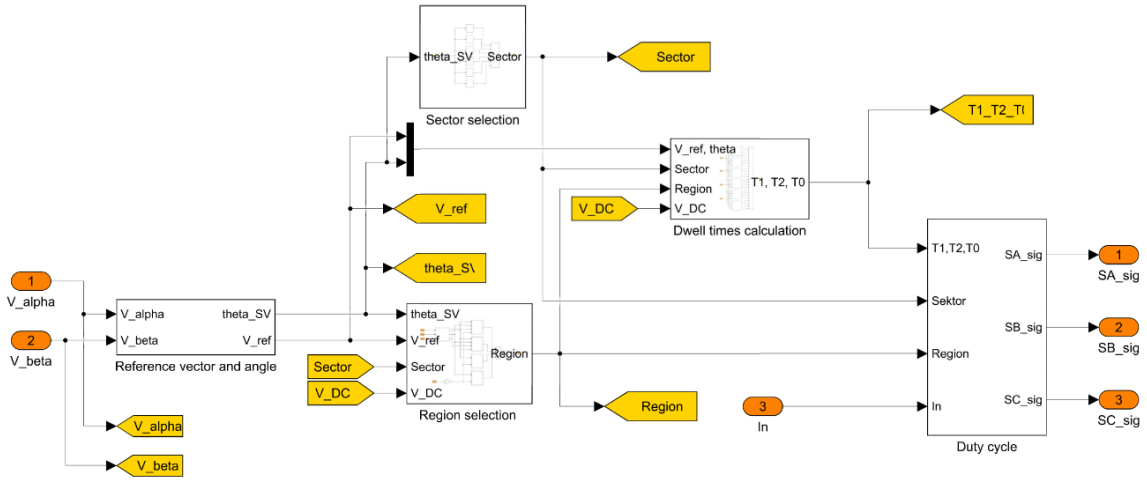

Fig. 16 SVPWM subsystem

6.7.1 Sector selection

Sector is chosen based on the angle of rotation θ (phase angle) of the reference vector. This is accomplished in the "*Sector selection*" subsystem, by transforming angle into degrees and then comparing it to sectors' limits. Because every sector has output either 0 or 1, the sector's output can be scaled to match the sectors number, i.e., sector four's output is multiplied by 4 to give 4 at the output. Results are then added to produce correct sector.

6.7.2 Region selection

In the three-level converter, there are 4 regions in every sector, assuming the NTV method is used. Depending on the magnitude and angle of the reference vector, vectors $\bar{V}_a$ and $\bar{V}_b$ are obtained using equations (5-7) and (5-8). By following the bounds of each region, described below these equations, the vectors are compared to select correct region. There is also a saturation block after the selection, to limit possible errors, when the reference vector is entering another sector.

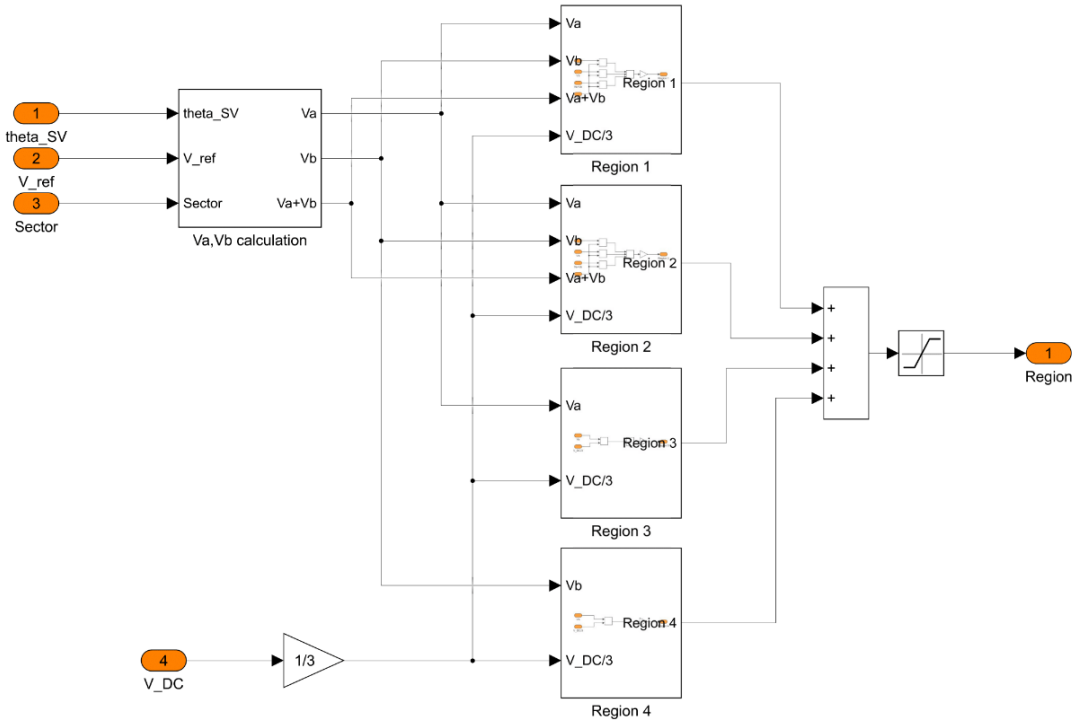

Fig. 17 Region selection

6.7.3 Dwell times

The dwell times are grouped together by the sector. In chapter 5.4.1 is shown the process of dwell time calculation for sector 1, also the final form of equations for sector 1 region 3 is presented there (equations (5-16) – (5-18)). The calculations process is same for every region of every sector, varying only in the equations used to obtain the dwell times.

6.8 Duty cycle

Final part of SVPWM is determining the duty cycles. Each leg is calculated separately, but the technique is the same. Duty cycles are calculated using the appropriate switching sequences, together with the dwell times to resemble the reference signal. There are two switching sequence options – Positive and Negative. Those two options are for voltage balancing which is explained in chapter 6.8.1. Reference signal is then compared with two triangle waves, to produce the modulated signal. Carrier waves are in a Phase Disposition order. Then there is a subsystem that takes the modulated signal and produces gates signals for switches in the converter's leg.

The gate signals are transformed in the "*Signal calculation NPC*" subsystem, which uses two Direct lookup tables to produce correct signal for each leg. Two Boolean inputs from the "*Modulation*" subsystem are converted into single value output from 0 to 3. These values represent the desired voltage level (P, 0, N) on the leg of the inverter. Then the "*Signal deciding*" lookup table selects the corresponding gate signals for the four switches in each leg.

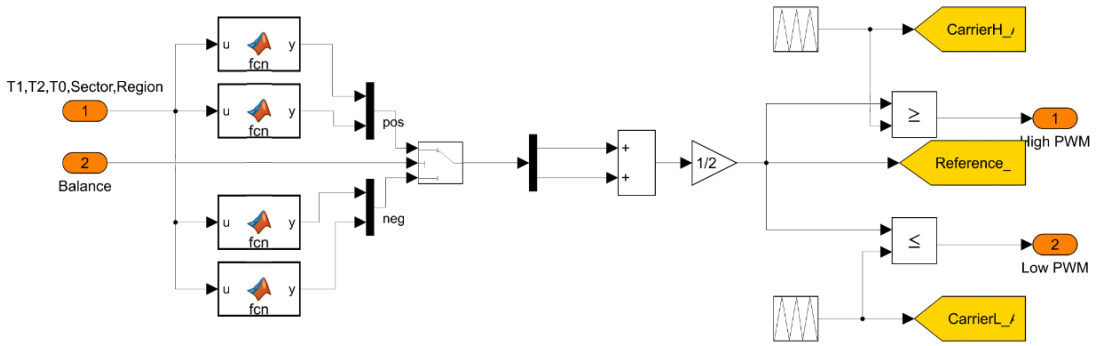

Fig. 18 Modulation subsystem for phase A

"*Precharging Switch*" subsystem controls the output gate signals for converter switches. If the capacitors are not fully charged, the output signals are given by the "*DC-link Precharging*" subsystem. When the capacitors are fully charged, switch flips and gate signals correspond to the duty cycles.

6.8.1 Voltage balancing

Effect of switching states on capacitors voltages is explained in chapter 5.4.1. To minimize the neutral point deviation, some kind of balancing technique must be implemented. This can be done passively by predetermining the switching sequence to utilize all vectors equally, or actively by measuring the voltage of the capacitors and accordingly selecting the space vectors to bring the deviance to zero.

Passive balancing is partly done in the NTV technique in regions 3 and 4. Because of only one small vector, the switching sequence can be divided to use positive and negative space vector for the same duration. Another method must be implemented for regions 1 and 2, for example symmetric modulation mentioned in chapter 5.4.2. However, this solves the balancing problem only partially. In a case that one voltage would drop significantly, this method cannot resolve the deviation and the voltages would remain unbalanced.

The voltage balancing can be solved by actively measuring the capacitors voltage and then determining which space vector should be used. Because all regions have at least one small

vector available to produce a switching sequence, the voltage can be balanced in every operational state. Then the vectors can be selected followingly:

- If neutral point is less than $V_{DC}/2$, positive space vectors are selected
- If neutral point is greater than $V_{DC}/2$, negative space vectors are selected

Because selecting positive space vectors causes the neutral current i_n flow into the neutral point, voltage on the upper capacitor will decrease and voltage on the lower capacitor will rise. Negative space vectors have opposite effect, causing the neutral current to flow out of the neutral point.

The previous techniques were implemented in the simulation model, by calculating both positive and negative switching sequences. Switching sequence is divided into 7 parts, which provides passive balancing for the regions 3 and 4. For regions 1 and 2 was implemented the active balancing approach.

In sector 2, there are two small vectors which makes the seven-segment pattern utilize more of positive or negative vectors. Assuming the sector 1 and region 2, if the overall output should be positive, meaning it should cause the neutral current to flow into the neutral point, the switching sequence would look like this:

$$\underset{(T_2/4)}{\bar{V}_2\,[0,0,N]} \rightarrow \underset{(T_0/2)}{\bar{V}_7[P,0,N]} \rightarrow \underset{(T_1/2)}{\bar{V}_1[P,0,0]} \rightarrow \underset{(T_2/2)}{\bar{V}_2\,[P,P,0]} \rightarrow \underset{(T_1/2)}{\bar{V}_1[P,0,0]} \rightarrow \underset{(T_0/2)}{\bar{V}_7[P,0,N]} \rightarrow \underset{(T_2/4)}{\bar{V}_2\,[0,0,N]}$$

This positive sequence represents the seven segments, where every step is active for half of the dwell time, except for the first and last step, where both are for one quarter of the dwell time, which makes it one half together. All vectors are equal to 1 in total, which obeys the equation (5-10). This utilizes the positive vectors for equal, or greater time than the negative vectors.

If the overall output should be negative, i.e., the neutral current flowing out of the neutral point, the switching sequence would look like this:

$$\underset{(T_1/4)}{\bar{V}_1[0,N,N]} \rightarrow \underset{(T_2/2)}{\bar{V}_2\,[0,0,N]} \rightarrow \underset{(T_0/2)}{\bar{V}_7[P,0,N]} \rightarrow \underset{(T_1/2)}{\bar{V}_1[P,0,0]} \rightarrow \underset{(T_0/2)}{\bar{V}_7[P,0,N]} \rightarrow \underset{(T_2/2)}{\bar{V}_2\,[0,0,N]} \rightarrow \underset{(T_1/4)}{\bar{V}_1[0,N,N]}$$

This negative sequence shows that the negative vectors are used for equal, or greater time than the positive vector.

The balancing technique is in the "*Voltage balancing*" subsystem, where "*Balancing table*" selects either positive or negative sequence to modulate the reference vector.

6.9 Neutral Point Clamped Converter

The NPC converter is constructed with the Simscape library. Rectified voltage from rectifier is fed to the $+V_{DC}$ and $-V_{DC}$ nodes where it supplies the converter. There are two capacitors C_1 and C_2 creating the converter's DC-link and neutral point in between them. The voltages of DC-link, both capacitors, and legs are measured here, together with neutral current and output phase currents. Twelve switches, four for each NPC leg, get gate signals from "*SVPWM*" subsystem.

6.10 Asynchronous machine

The induction motor, which is supplied by the NPC converter, is from the Simscape library. It is a squirrel cage induction motor with parameters presented in Table 3. It was selected, due to the difference between the Simulink and Simscape library and their compatibility. To verify that the motor from the Simscape library behaves according to the system of equations for the motor, a mathematical motor was constructed. The mathematical motor was then used to verify the accuracy.

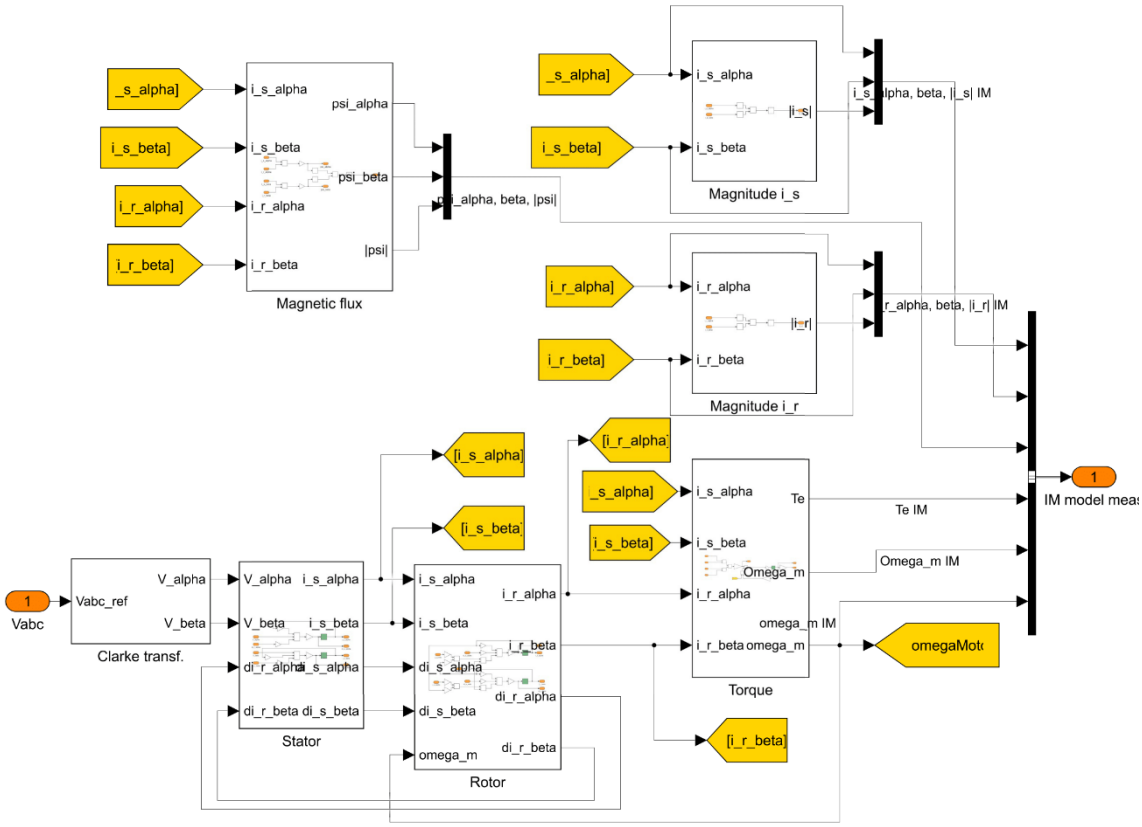

Fig. 19 Mathematical model of the induction motor

6.11 Mathematical model of the Induction Motor

This mathematical model uses equations (4-18) – (4-23) to simulate the motors behavior. Stator current quantities from equations (4-18) and (4-19) are calculated in the "*Stator*" subsystem, similarly in the "*Rotor*" subsystem, the rotor current quantities are obtained using equations (4-20) and (4-21). Motor's torque is calculated in the "*Torque*" subsystem together with the rotor speed from equations (4-22) and (4-23). The "*Magnitude*" subsystems obtain a magnitude of stator current and rotor current and are used as an informational tool. Magnetic flux is acquired through the "*Magnetic flux*" subsystem, which also calculates its magnitude. Values obtained from this model are then used to approximately compare both motor models.

Because the NPC model was constructed with Simscape library, its output voltage feeds the Simscape IM from the same library. The implemented control techniques then take the values (feedback) from the Simscape models and use it for other calculations. This mathematical model is therefore inaccurate when it is being controlled with feedback methods. However, it is still being powered from the NPC converter voltage, using a conversion between the libraries. Unfortunately, this works only one way.

6.12 Parameters

Table 3 Parameters of the squirrel cage induction motor

$P_n = 2\ 250$ HP	Nominal power
$\cos\varphi = 0.8$	Power factor
$V_n = 2.4$ kV	Nominal line-to-line voltage
$f_n = 60$ Hz	Nominal voltage
$n_n = 1794$	Nominal speed
$p_p = 2$	Number of pole pairs
$R_s = 0.029\ \Omega$	Stator resistance
$R_r = 0.022\ \Omega$	Rotor resistance
$X_{ls} = X_{rs} = 0.226\ \Omega$	Stator, rotor leakage reactance
$X_m = 13.04\ \Omega$	Magnetizing reactance
$J = 63.87\ \text{kg} \cdot \text{m}^2$	Moment of inertia
$T_n = 8\ 935$ N m	Nominal torque
$B = 5.879 \cdot 10^{-3}$ N m/(rad/s)	Friction coefficient

Because some of these parameters are required in different form, they can be transformed using these formulas:

$$P_n(\text{kW}) = P_n \cdot 0.746\ (\text{HP}) \tag{6-7}$$

$$L_{ls}\ (\text{H}) = \frac{X_{ls}}{2\pi \cdot f_n}\ (\Omega) \tag{6-8}$$

7 Simulation Results

There is a lot of possible options how to conduct the simulation. To show that the model is functional, there will be shown three control methods, showing the VSD's operation.

7.1 Simulation of Scalar Control

Simulations were conducted using the SVPWM with phase disposition of the triangle carriers. Modulation index reached $M = 0.889$ at the top speed and frequency ratio was set to $P = 187.5$. Reference speed values were given as +800 rpm, +1 600 rpm and +1 200 rpm with no load. In the range of 1.8 to 2.5 sec, the motor was loaded with 4 000 N m.

7.1.1 Open-loop control

The presented figures show the rotor speed slowly increasing up to 800 rpm with slight overshoot, and then rising to 1 600 rpm also with overshoot. Although it is hard to recognize from the graph in Fig. 20, the rotor speed decreases when load torque is applied. Another overshoot is when the rotor speed is reduced. These overshoots are caused by the lack of the feedback loop, which can be observed when other control techniques are presented.

At the beginning, the currents are above the nominal values, which could cause problems over extended period. These high currents are caused by the precharging of the capacitors and by the V/f control in the low speed region. The low speed region is limited to 10 % of the nominal frequency to sustain stability of the scalar control mentioned in chapter 4.2.1. When the reference speed is reached, the currents drop, until the motor is loaded. Reducing the voltage to reduce the rotor speed, causes the currents to rise, until the speed settles again.

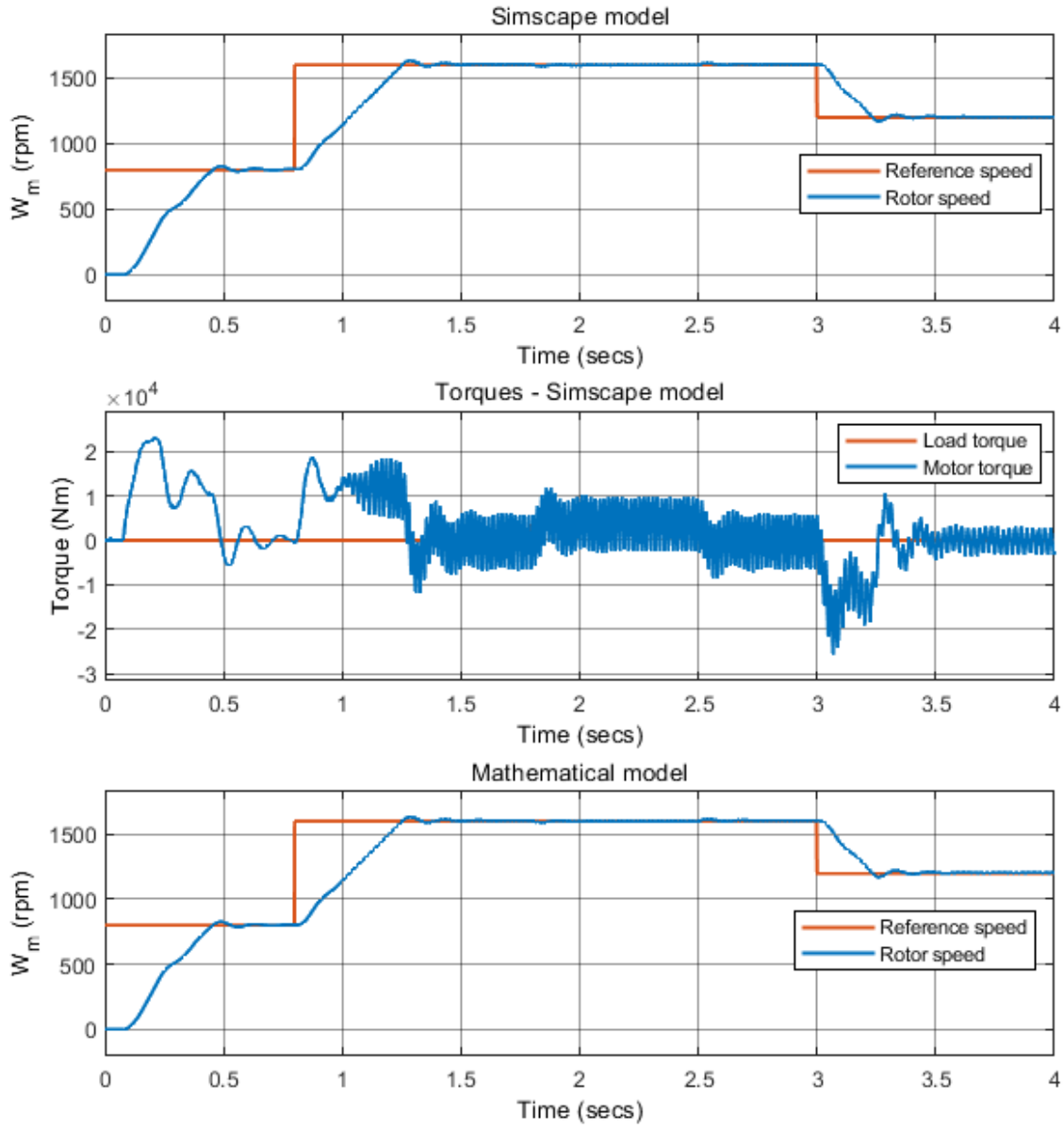

Fig. 20 Rotor speed and torque of the Open-loop control

As the voltage increases, the reference space vector is rotating faster, and its magnitude rises. This can be seen through the phase angle, and selected sectors and regions. Higher frequency causes faster rotation of the phase angle, thus faster sector selection. Increasing magnitude causes selection of regions that are farther away from the origin. Therefore, at the start of the simulation, only region 1 is selected. When the voltage is maximal, regions 3 and 4 are selected.

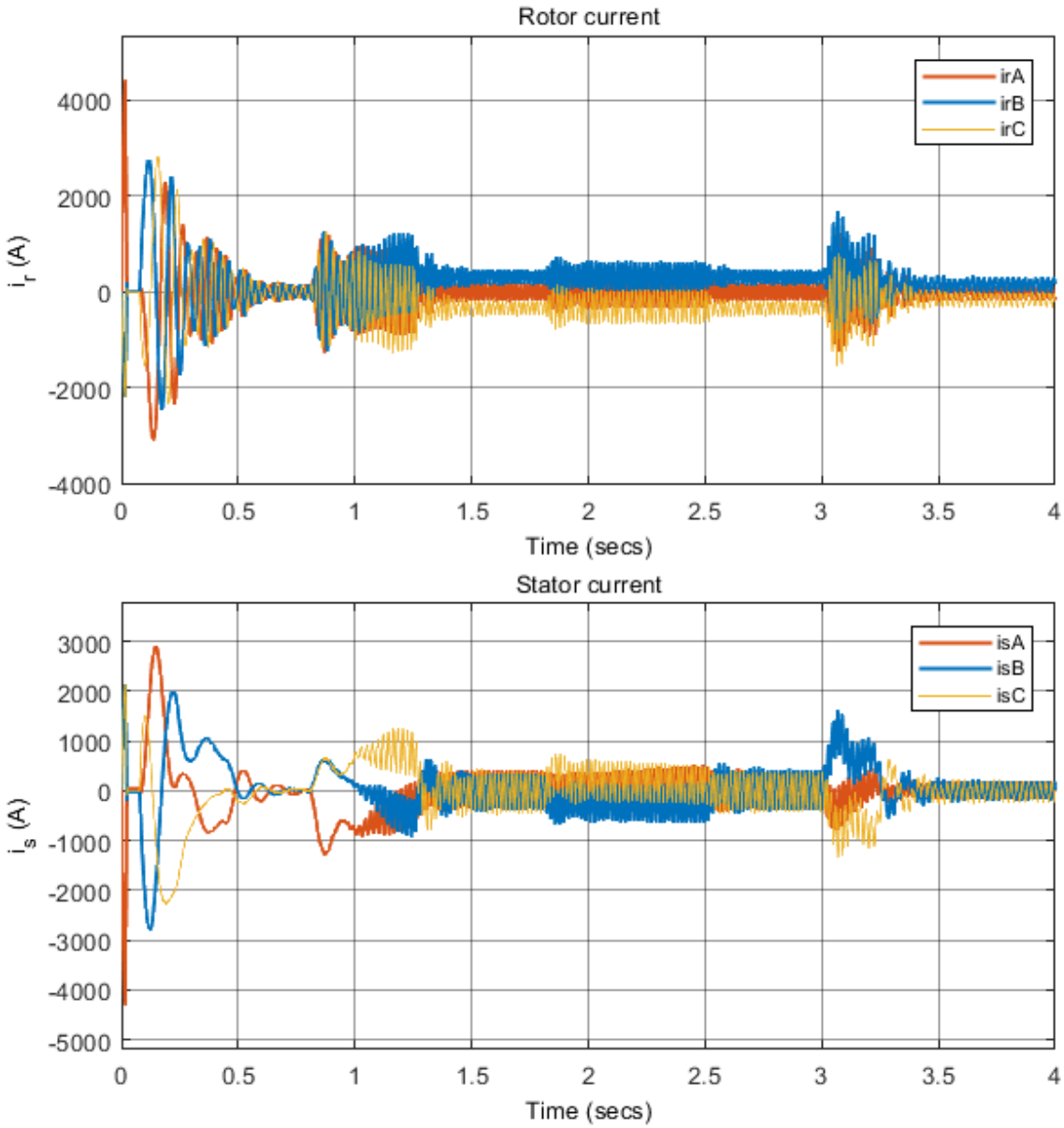

Fig. 21 Rotor and stator currents of the Open-loop control

The measure voltages show how the original reference voltage is modified by the SVPWM method, that the NPC converter outputs line-to-neutral voltage as shown in Fig. 22. Because of the V/f limit at the beginning, the reference voltage is constant. The A output voltages of the NPC show, that at the beginning there is some non-zero voltage. This is because of the capacitors precharging, and it ends quickly. In the precharging subsystem is a deciding process, that determines if V_{C1} is greater than V_{C2}. If this is true, the leg A will be switched to have positive output and legs B, C will have zero output. The magnitude of the reference vector, thus the value of the NPC's output voltage, can be seen from the amplitude of the reference vector and from the levels of the line-to-neutral voltage. When the magnitude is low, amplitude is low and l-to-n voltage is changing only between three levels. When the voltage is high, the magnitude is bigger and the l-to-n voltage is changing between five levels.

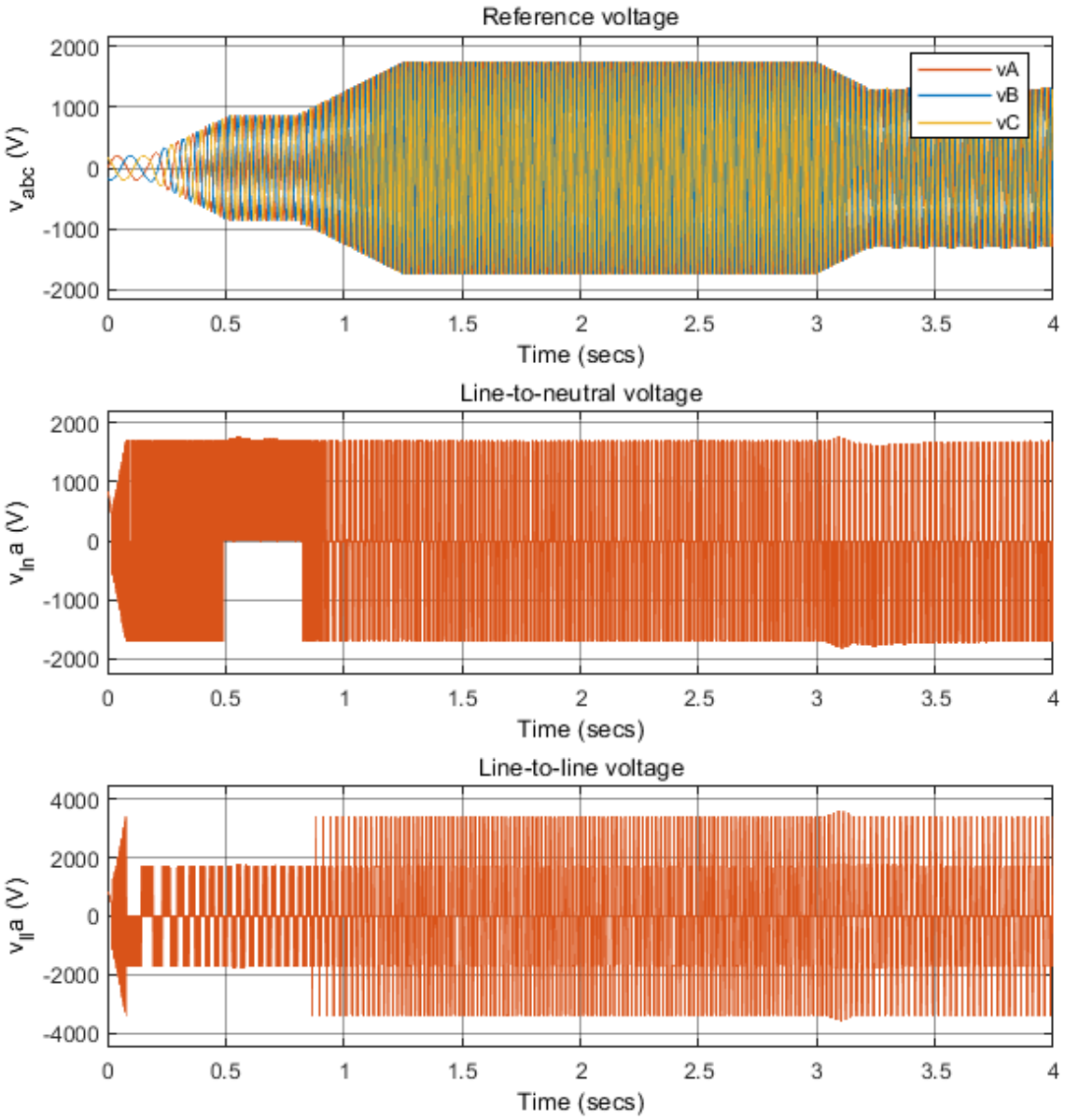

Fig. 22 Reference and NPC converter voltage of the Open-loop control

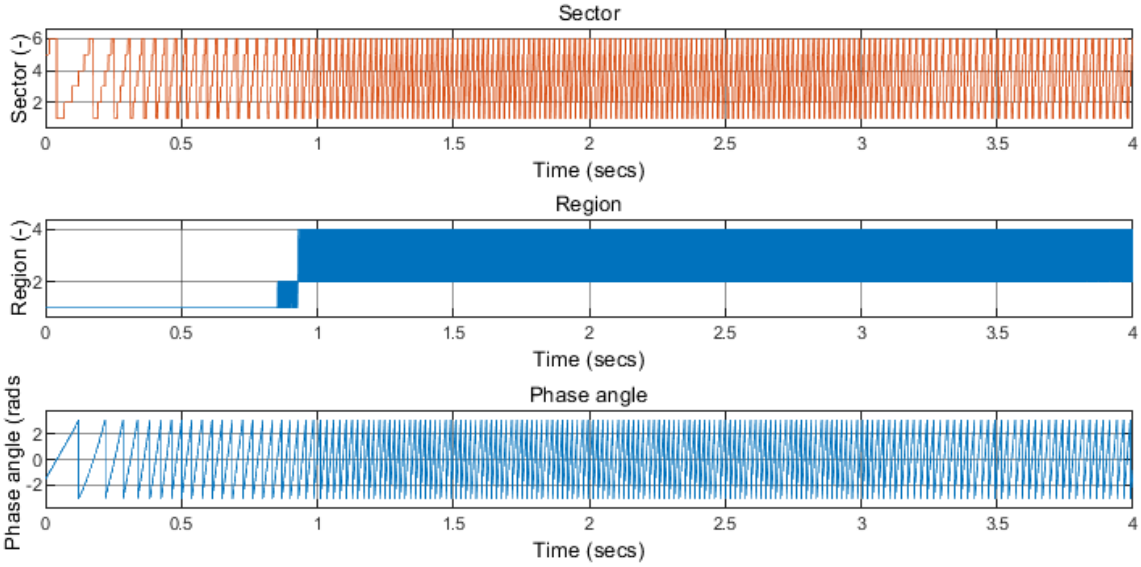

Fig. 23 Sector, region and phase angle of the Open-loop control

The capacitors voltage remains almost same for most of the simulation. At the start of the simulation, voltages converge and then begin to charge together. This can be seen in the close-up in Fig. 25. After reaching the value of $V_{DC}/2$, the voltages are at the same value until negative torque is introduced. Every time, the torque drops below zero, voltages deviate. However, after the torque reaches positive values, the voltages converge.

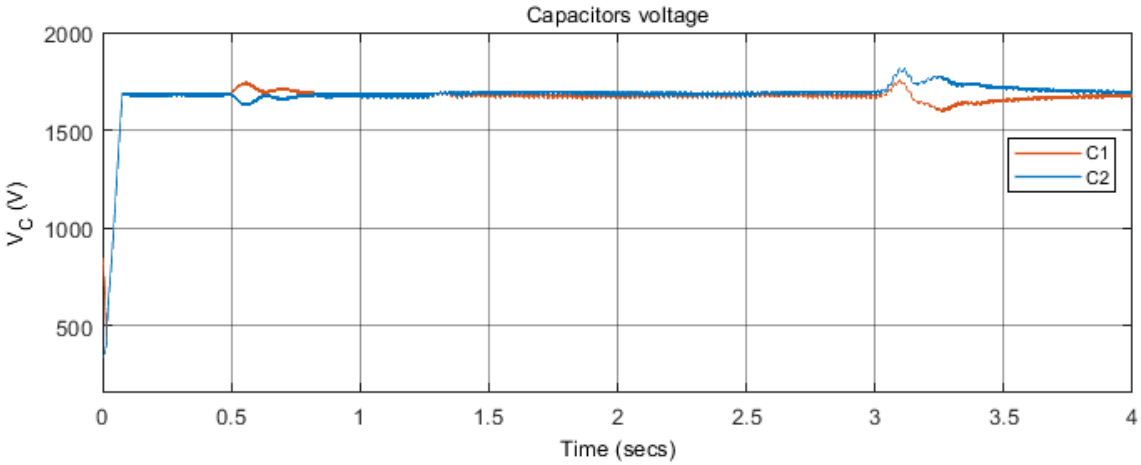

Fig. 24 Capacitors voltage of the Open-loop control

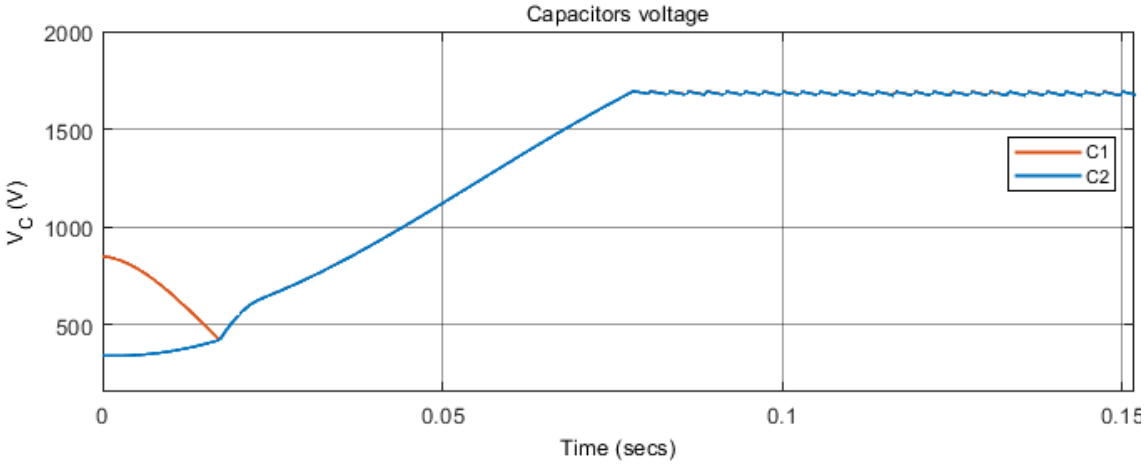

Fig. 25 Close-up of charging of the capacitors of the Open-loop control

7.1.2 Closed-loop Control

The closed-loop control is not much different from the open-loop control. The graphs are zoomed in, to give better perception of the scalar control simulation. The simulation follows the same order and timing of the reference values, as it was for the open-loop control. The speed rises to reference values with minimal overshoots. Only when the speed is decreased, the overshoot is significant. In Fig. 26 is shown the decrease of rotor speed, due to loading from 1.8 to 2.5 sec.

In the graphs in Fig. 28 are clearly visible the output voltage levels of the NPC converter. Also the reference voltage is clearly constant until time 0.8 seconds, when new reference speed is executed.

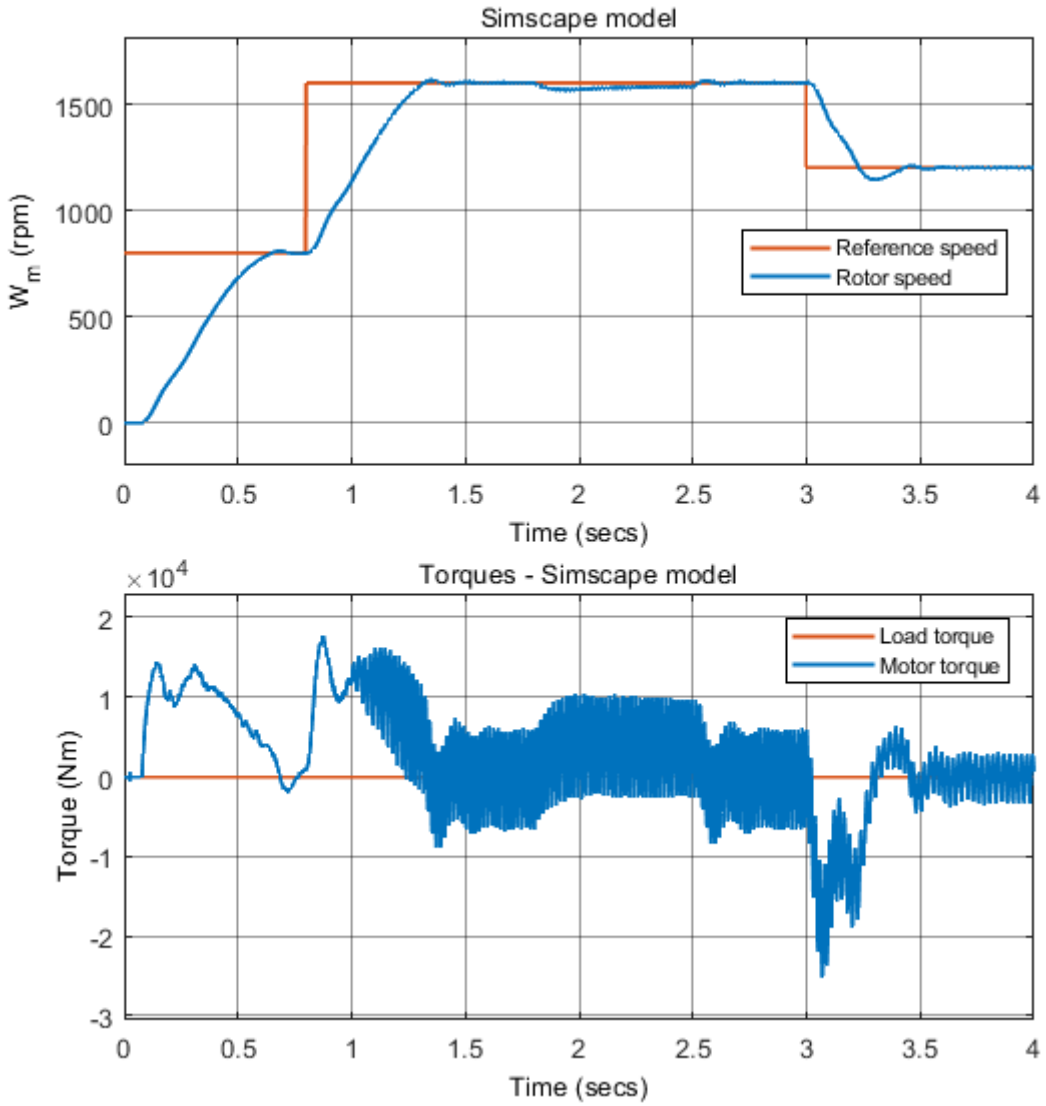

Fig. 26 Rotor speed and torque of the Closed-loop control

The graph with the voltage of the capacitors shows, that the overcharge is less than it was during the open-loop control and that the curve is similar to the curve of previous method.

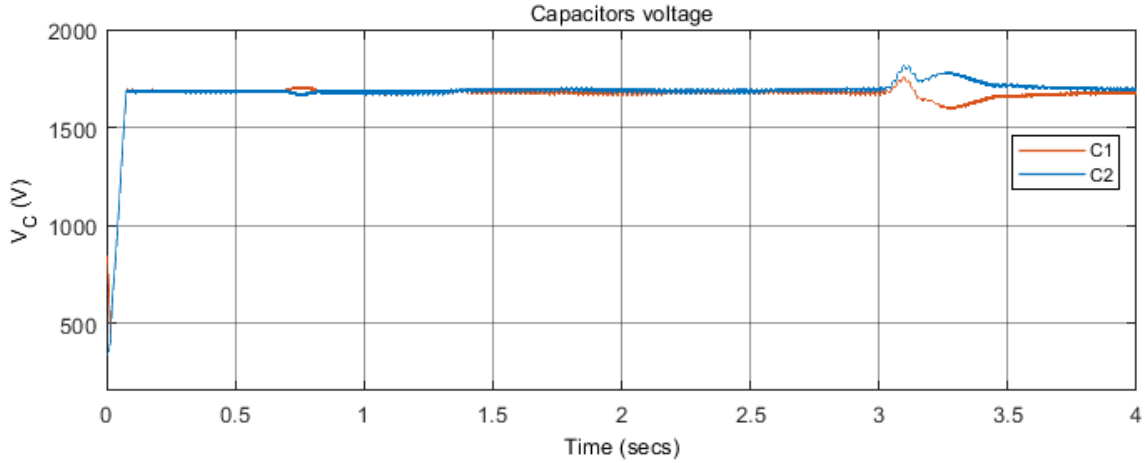

Fig. 27 Capacitors voltage of the Closed-loop control

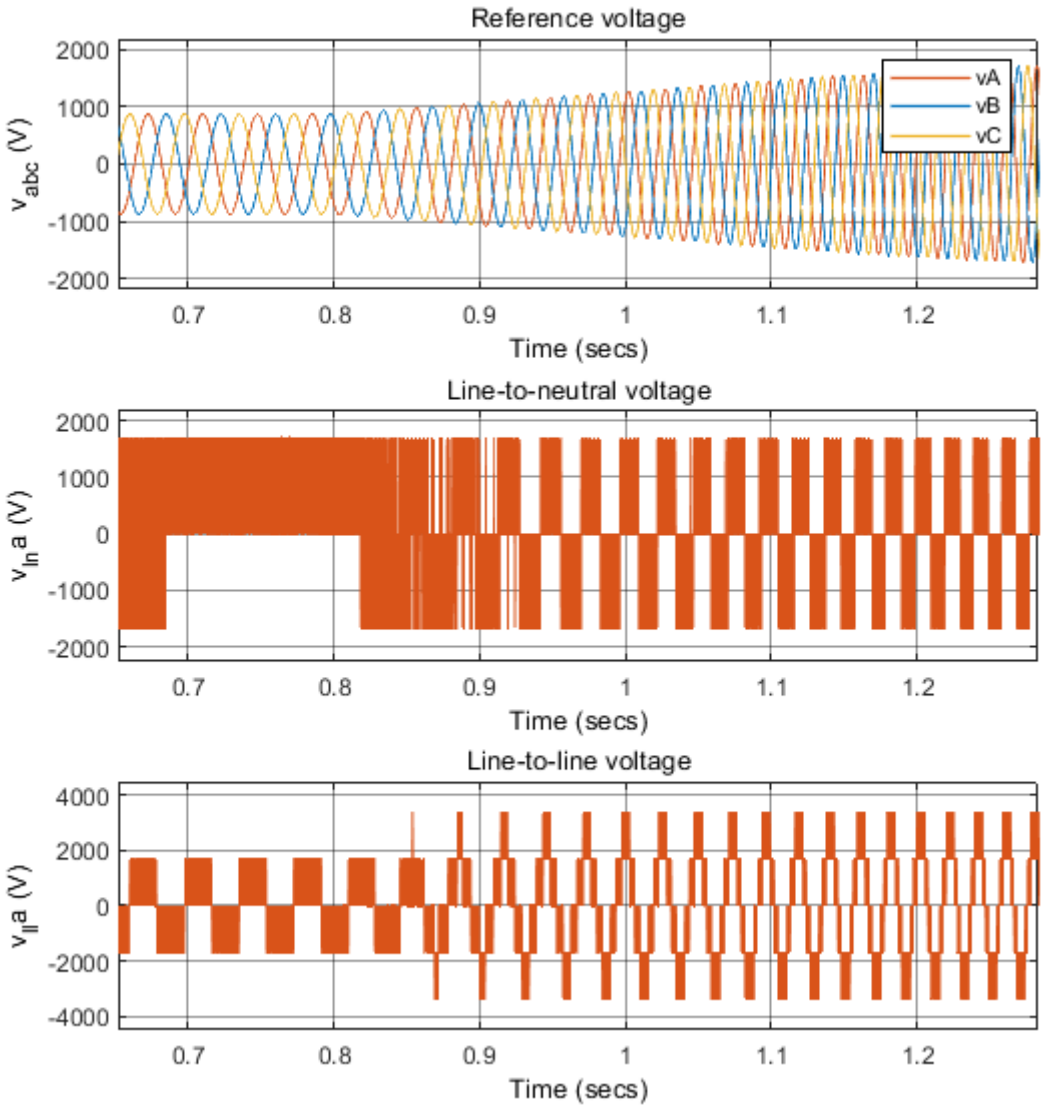

Fig. 28 Reference and NPC converter voltage of the Closed-loop control

7.1.3 Scalar control differences

Because open-loop control has no feedback it is harder to control the speed of the rotor. The torque oscillates more which causes oscillation of the rotor. This can be seen if the Fig. 20 is compared with Fig. 26. Closed-loop control is steadily increasing the rotor speed without big jumps during the first and second rise. Although, the torque does not exceed 2 000 N m, rotor reaches the speed of 800 rpm almost at the same time. The big difference is that while open-loop control had overshoots, closed-loop control can increase the voltage without any overshoots.

Another difference is the overcharge on capacitors. Closed-loop control performs better, and the first voltage deviation around 0.5 seconds is approximately 2 times smaller, than the deviation of open-loop control.

7.2 Simulation of Vector Control

The possibility of controlling torque and flux independently should provide better control than having the field components coupled. This can be seen from the presented figures. Although the speed of the rotor was slower compared to the scalar control, other qualities are significantly better. The simulation was conducted similarly to the scalar control simulation, but reference speeds and load were given at later time. Also, the capacitors were fully charged at the start. Because the motor quantities were in steady state, both scalar and vector control should be comparable. The *dq* current control was used to estimate the rotor flux during the simulation.

Fig. 29 shows the rotor speed smoothly increasing up to 800 rpm and up to 1 600 rpm, and smoothly decreasing to 1 200 rpm. From 2 to 2.5 seconds, the motor is loaded with 4 000 N m. A decrease in motor speed, due to loading is in Fig. 32.

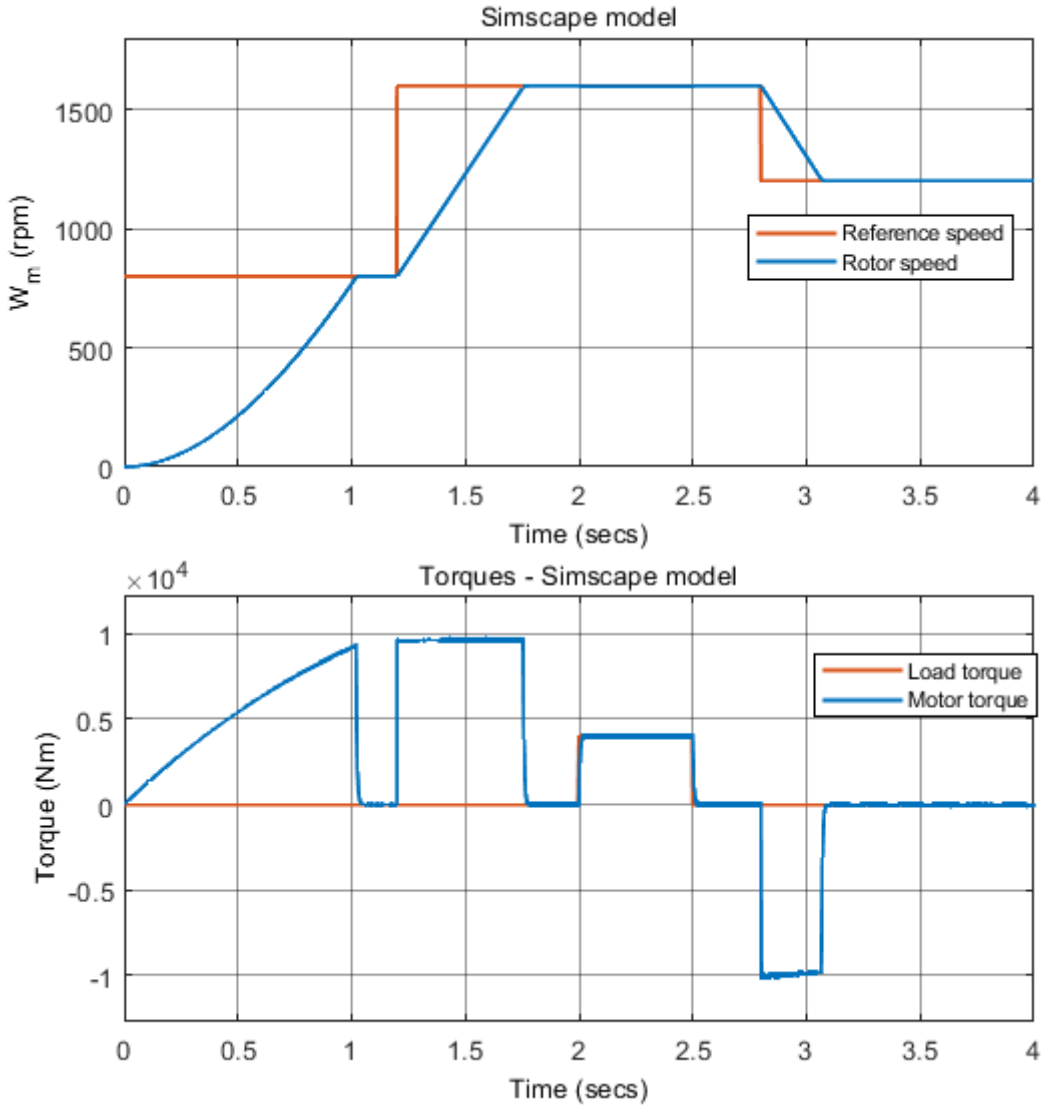

Fig. 29 Rotor speed and torque of the Vector control

The torque is also changing smoothly without any jumps or oscillations. Because the model was built to respect the maximal current flow, the dq components of stator current were limited, which limited the torque. If those limits were set higher, or completely removed, the torque could be higher and the rotor would reach the reference speed quicker.

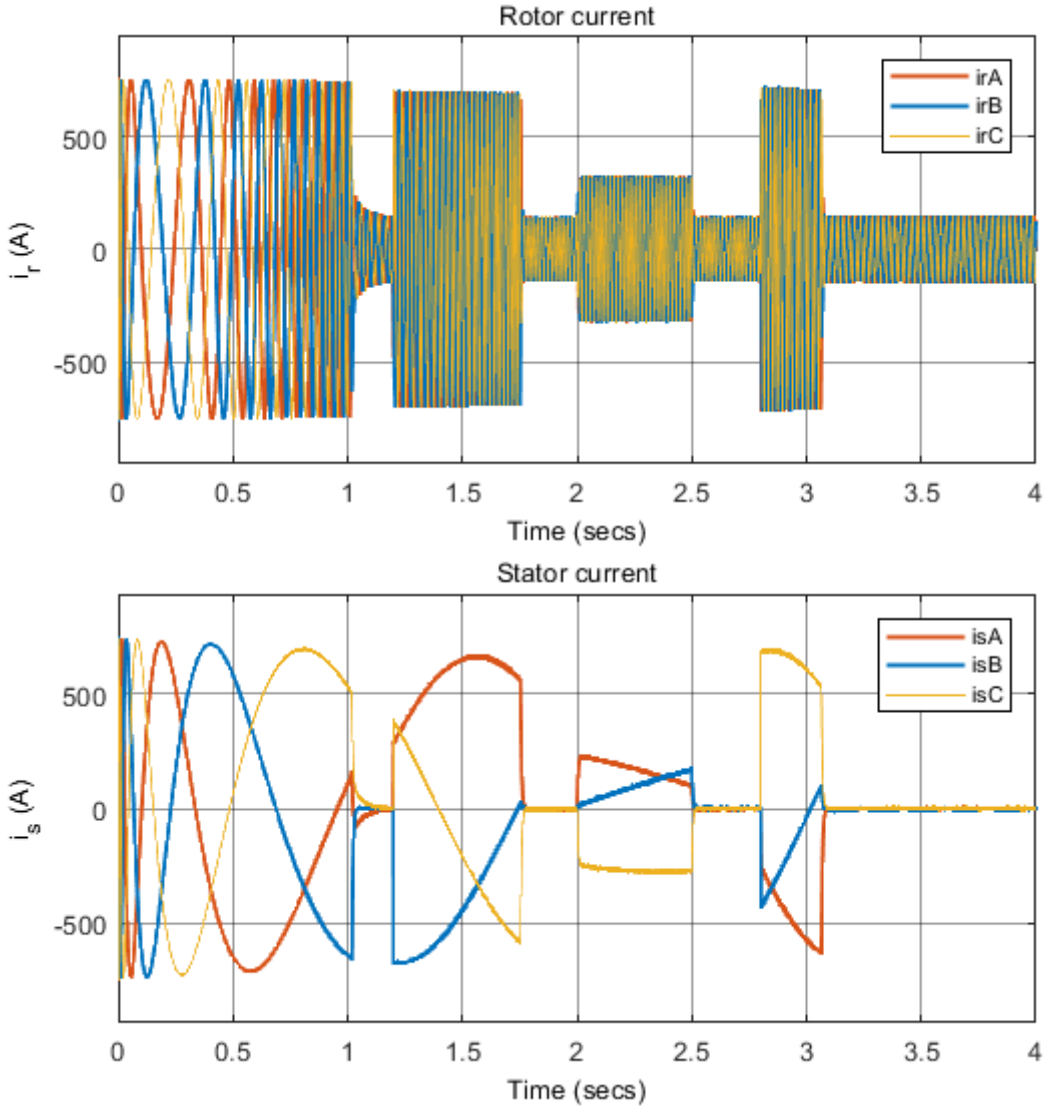

Fig. 30 Rotor and stator currents of the Vector control

The current limits can be seen in Fig. 30, where the currents do not exceed 700 A. At the beginning the currents aplitudes are at their limit and the frequency is small, which is similar to scalar control. The frequency increases together with the rotor speed, but the amplitudes are still limited.

The reference voltages' amplitude and the frequency are increased gradually, which causes the reference vector to gradually increase rotation and magnitude. Line-to-neutral voltages, the voltages at the output of the converter, are being switched in three levels ($\pm$ 1 697 V and 0 V). Switching between values $\pm$ 1 697 V, which is the value of half of the DC-link, has to go throgh the 0 value first. This is in order to prevent excessive stress that would be put on the converter parts. This is especially important when dealing with medium- or high-voltage multilevel converters.

The line-to-line voltage is changing between five levels. This is because each of the opposed lines can have 3 voltage levels, with zero voltage being the middle.

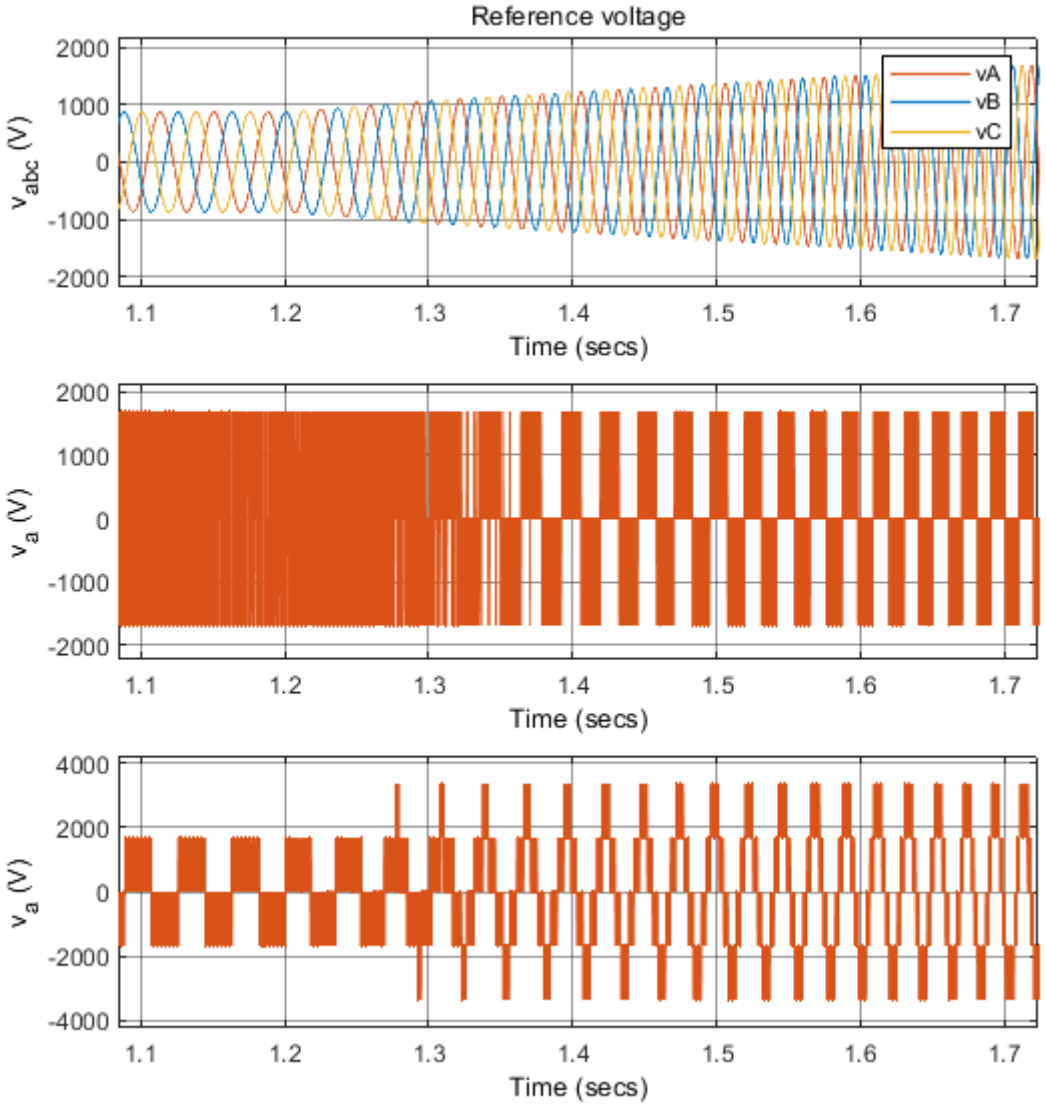

Fig. 31 Reference and NPC converter voltage of the Vector control

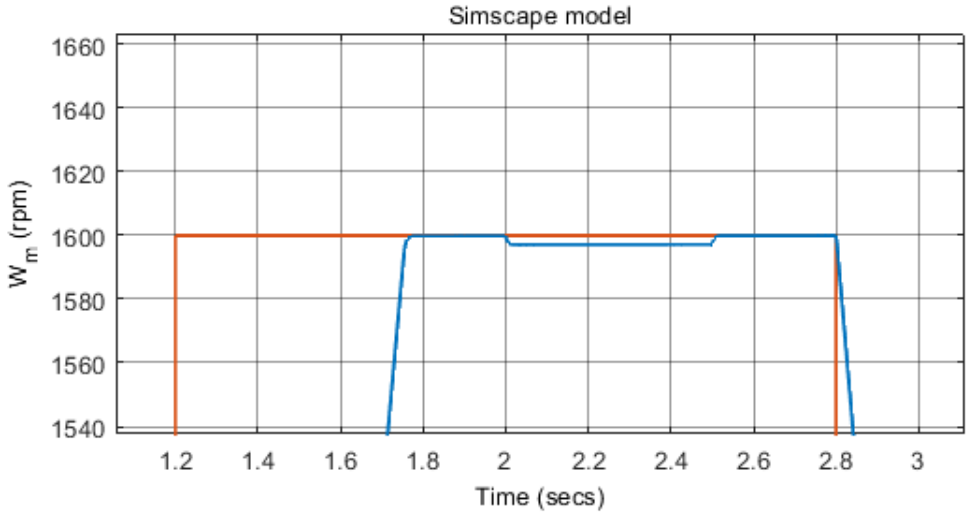

Fig. 32 Close-up of the rotor speed of the Vector control

The capacitors voltage is equal to $V_{DC}/2$ for most of the time, until the torque is negative and the voltages deviate similarly as it was in the scalar control.

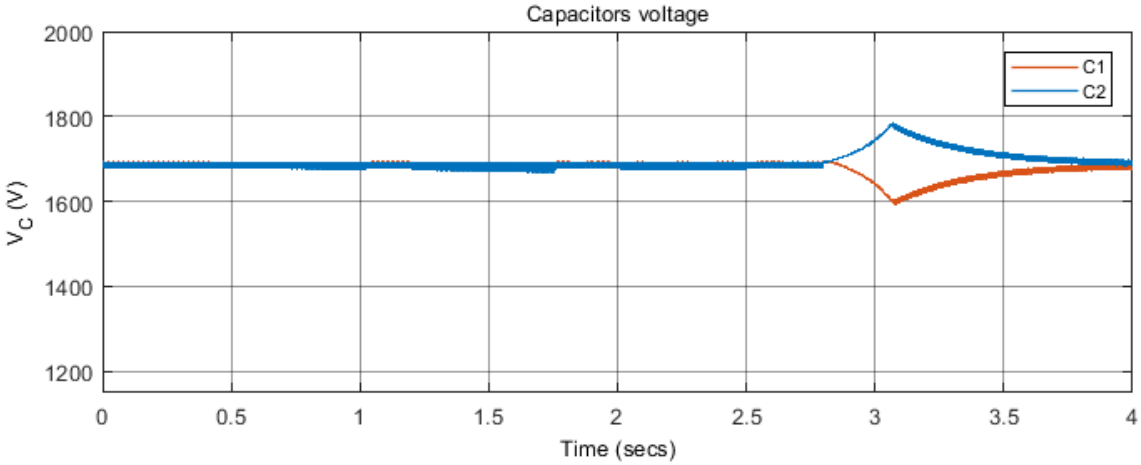

Fig. 33 Capacitors voltage of the Vector control

7.3 Simulation of Voltage Balancing

The model implements a precharging subsystem, to balance voltages of the capacitors and therefore provide optimal starting point for the NPC converter. While the converter is running, passive and active balancing technique is in function, to minimize the neutral point deviation.

As shown in Fig. 24 and Fig. 27, the capacitor voltages are being equalized and then charged to the value of half of the DC-link. The voltages oscillate with the load but remain equal. There is considerably big deviation around 0.7 sec, when motor torque is negative and neutral current is positive. Another big deviation is around 3.25 sec, when the torque is again negative, but neutral current is this time negative.

Fig. 34 shows the operation under same circumstances as the simulation process for vector control, but no active balancing is implemented. This causes the voltage to deviate when the reference vector lies in regions 1 and 2. Passive balancing prevents further deviation.

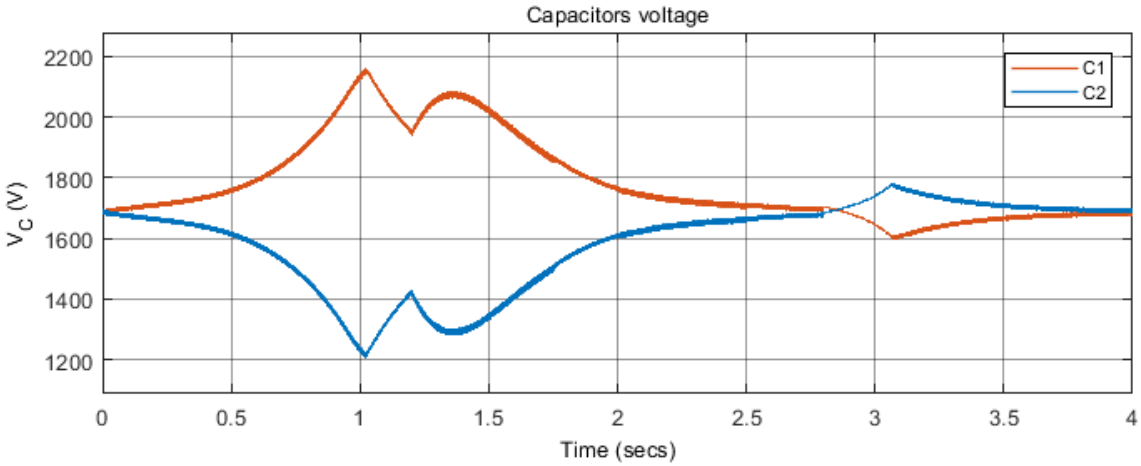

Fig. 34 Capacitors voltage without voltage balancing

7.4 Simulation of SVPWM

The previous controls have variable amplitude and frequency. This means that the modulation index and the frequency ratio were changing throughout the simulation. For rotor speed of 1 400 rpm, the index was at $M = 0.889$ and ratio at $P = 187.5$, graph with the reference vector and carriers is in Fig. 35. Because the carrier frequency is high and graphs are hard to read, another simulation was conducted, with carrier frequency of 1 000 Hz and modulation index set at $M = 1$. The reference signal frequency was kept constant at 60 Hz, which means that frequency ratio was $P = 30$.

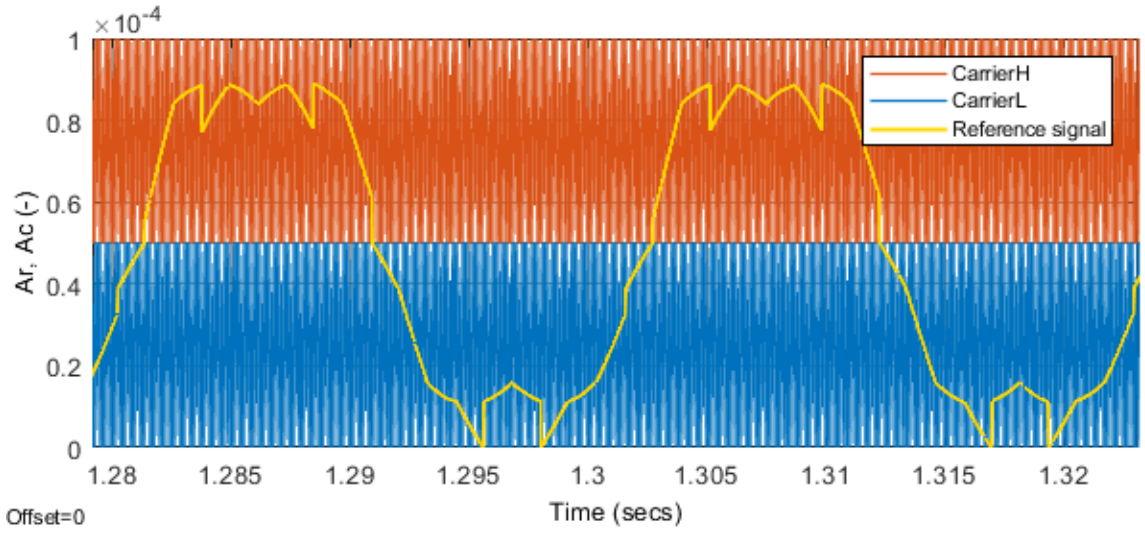

Fig. 35 Carrier and reference signals, M = 0.889, P = 187.5

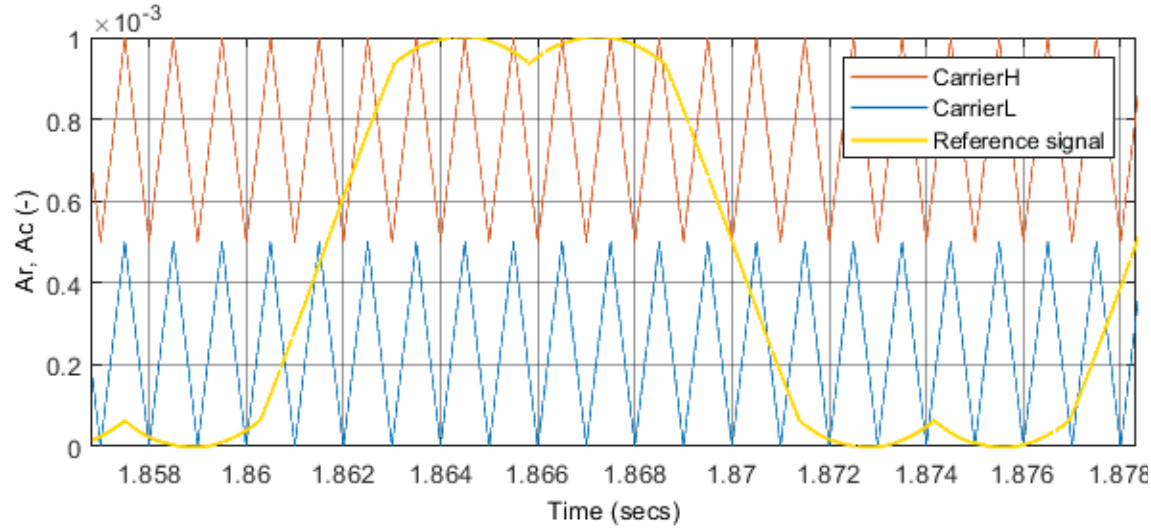

Fig. 36 Carrier and reference signals, M = 1, P = 30

The reference signal is significantly deformed, when the modulation index is low. This is obvious from the graph in Fig. 35. Further decrease of the modulation index would cause bigger deformation of the reference signal. Decreasing the modulation index causes also causes lower content of the fundamental frequency. The second figure shows intentionally deformed reference signal, in order to increase the content of the fundamental frequency.

8 Conclusion

The first part of the of the thesis topic was to introduce the possible control techniques of multilevel converters for variable speed drives. The control methods of converters were presented in the chapter 5 and special attention was given to the PWM and SVPWM method, because these methods are the most common and are not hard to implement. Because the SVPWM method was used in the simulation, the nearest three vector method was presented. Downfall of this method is voltage balancing, that had to be worked out, in order to keep the capacitors' voltage levels at the same value.

Because the output voltage is not easy to read, the induction motor was introduced in chapter 4. Converter feeds the motor, and if there would be any mistake in the simulation, it should be obvious in the motor's performance. Induction motor is simple to simulate, especially the squirrel cage induction motor, therefore this motor was used for simulations.

The control techniques used for the control of induction motor were also presented. Because there is a lot of possible qualities, that could be tracked and followed, only few main were selected. The rotor speed and torque, together with the motor currents were used to compare the techniques.

Second part of the thesis topic was to make appropriate simulation model of a converter. The chosen converter was the three-level three-phase neutral point clamped converter, which was successfully created in the MATLAB Simulink environment, using the Simscape library. Because of this library, Asynchronous motor, from the Simscape library had to be picked, to properly simulate the control techniques.

Third part was to create a suitable control strategy for the control of the converter. The control technique consisted of SVPWM modulation, with the use of the nearest three vector technique. Because of neutral point deviation, another control technique had to be introduced, to keep the voltages steady. From the presented passive and active methods, a combination of both was implemented, which is described in chapter 6.8.1.

This balancing method kept voltages at the same value, which was demonstrated by omitting the balancing algorithm and using only the NTV technique.

Last part of the thesis topic was to conduct simulations to verify the function of the simulated model and evaluate the results. The conducted simulations were for open-loop scalar control, closed-loop scalar control and field oriented vector control. In all of these types of control the motor performed adequately, but there were some differences.

The comparison of the conducted simulations is in chapter 7. Because the open-loop and closed-loop controls are similar, they were compared together to show the differences.

From the results it can be said that the vector control outperforms the other types of control. This is mainly due to the fact, that the torque is behaving very smoothly, compared to scalar control. During the simulation, only one overshoot occurred, which caused the capacitors voltage to deviate. Also, the rotor and stator currents were much better. If the charging currents were dismissed, because they were not simulated for the vector control, the vector control currents did not exceed the nominal values, which were set before the simulation. Unlike the scalar control, where the currents in the low speed region were almost 4-times bigger.

On the other hand, the speed it took to reach the reference speed was the worst in vector control and best in open-loop control. However, the difference was only few hundred milliseconds. This difference is most likely caused by the limit of the stator current. Because open-loop control had no limit and only performed on the $V/f = const.$ ramp it could produce more torque.

The modulation technique used had two factors that could be tracked. Because all three types of motor controls had same outcomes, there was nothing to compare between them. But to show the difference, a simulation with high modulation index and lower modulation index were presented, which showed the deformation of the reference vector, resulting in worse output voltage of the NPC converter.

The voltage balancing was a great way to show the difference between the types of converter control strategies. If the neutral point voltage was neglected, the NPC converter had same output voltage as if the voltage balancing was considered. However, the deviation was enormous and it could not be used outside of simulation in practice.

To conclude the thesis, it can be said, that from the simulated methods and techniques, the SVPWM modulation, together with some active voltage balancing, is a good choice to control the three-level three-phase NPC converter and vector control, specifically field oriented control, is superior to scalar control.

References

[1] ABB, "Drives," ABB Asea Brown Boveri Ltd, [Online]. Available: https://new.abb.com/drives/what-is-a-variable-speed-drive. [Accessed 11 - 11 - 2022].

[2] S. M. M. A. A. S. H. M. R. Saidur, "Applications of variable speed drive (VSD) in electrical motors energy savings," *Renewable and Sustainable Energy Reviews,* vol. 16, no. 1, pp. 543-550, 2012.

[3] G. Takacs, Electrical Submersible Pumps Manual (Second Edition), Gulf Professional Publishing, 2018, pp. 153-240.

[4] M. Barnes, Practical Variable Speed Drives and Power Electronics, M. Barnes, Ed., Oxford: Newnes, 2003, pp. 1-35.

[5] ABB, "Technical guide No. 4," 2011. [Online]. Available: https://library.e.abb.com/public/d3c711ec2acddb18c125788f002cf5da/ ABB_Technical_guide_No_4_REVC.pdf. [Accessed 15 - 12 - 2021].

[6] P. Kobrle, "Control strategy of five-level flying capacitor inverter," Ph.D. Dissertation, Czech Technical University in Prague, Prague, 2014.

[7] P. T. Krein, "1 - Introduction," in *Power Electronics Handbook (Third Edition)*, Third Edition ed., M. H. Rashid, Ed., Boston, Butterworth-Heinemann, 2011, pp. 1-14.

[8] I. B. E. International, "CHAPTER 7 - Motors," in *Electrical Systems and Equipment (Third Edition)*, Oxford, Pergamon, 1992, pp. 623-648.

[9] Siemens, "SINAMICS Medium Voltage Converters," Siemens AG, Nuremberg, 2021.

[10] M. Matteini, "Control Techniques for Matrix Converters," Ph.D. Dissertation, University of Bologna, Bologna, 2001.

[11] M. F. N. H. P. Yam P. Siwakoti, "Chapter 1 - Power Electronics Converters—An Overview," in *Control of Power Electronic Converters and Systems*, F. Blaabjerg, Ed., Academic Press, 2018, pp. 3-29.

[12] A. R. Strandt, Comparison of Three Space Vector PWM Methods for a Three-Level Inverter with a Permanent Magnet, Milwaukee: Master's Thesis, Faculty of the Graduate School, Marquette University, 2013.

[13] J. S. Lai and F. Z. Peng, "Multilevel converters-a new breed of power converters," in *IAS '95. Conference Record of the 1995 IEEE Industry Applications Conference Thirtieth IAS Annual Meeting*, vol. 3, 1995, pp. 2348-2356.

[14] Y. Jiao, "High Power High Frequency 3-level Neutral Point Clamped," Ph.D. Dissertation, Virginia Polytechnic Institute and State University, Blacksburg, 2015.

[15] T. &. B. S. Bruckner, Loss balancing in three-level voltage source inverters applying active NPC switches, 2001 IEEE 32nd Annual Power Electronics Specialists Conference (IEEE Cat. No.01CH37230), 2001.

[16] S. C. G. K. J. P. a. R. P. A. M. A. Perez, Modular Multilevel Converters: Recent Achievements and Challenges, IEEE Open Journal of the Industrial Electronics Society, vol. 2, pp. 224-239, 2021, 2021.

[17] S. Debnath, J. Qin, B. Bahrani and M. Saeedifard, "Operation, Control, and Applications of the Modular Multilevel Converter: A Review," *IEEE Transactions on Power Electronics,* vol. 30, no. 1, pp. 37-53, 2015.

[18] M. Baazouzi and F. Bacha, "Control Strategy of Modular Multilevel Converter: theoretical investigation and performance," in *2019 International Conference on Signal, Control and Communication (SCC)*, 2019, pp. 296-301.

[19] Rockwell Automation Inc., "PFLEX-BR010E-EN-P – June 2021," 06 2021. [Online]. Available: https://literature.rockwellautomation.com/idc/groups/literature/documents/br/pflex-br010_-en-p.pdf?event-category=Brochure&event-action=Download&event-label=PowerControl_Global_XX_EN_2016_Medium_Voltage_Dri. [Accessed 15 - 12 - 2021].

[20] Rockwell Automation Inc., "PowerFlex 6000 Medium Voltage AC Drives | Allen-Bradley," [Online]. Available: https://www.rockwellautomation.com/en-us/products/hardware/allen-bradley/drives/medium-voltage-ac-drives/powerflex-6000-ac-drive.html. [Accessed 07 - 01 - 2022].

[21] Toshiba International Corporation, "Motors, Drives, Controls, & PLCs Catalog," Houston, 2022.

[22] TMEIC, "Medium Voltage AC Drives," Toshiba Mitsubishi-Electric Industrial Systems Corporation, [Online]. Available: https://www.tmeic.com/products/medium-voltage-ac-drives. [Accessed 18 - 02 - 2022].

[23] P. J. Kobrle Pavel, Elektrické pohony a jejich řízení, Prague: CVUT Praha, 2016.

[24] R. J. Lee, P. Pillay and R. G. Harley, "D,Q reference frames for the simulation of induction motors," *Electric Power Systems Research,* vol. 8, no. 1, pp. 15-26, 1984.

[25] J. A. Dittrich and N. P. Quang, Vector Control of Three-Phase AC Machines: System Development in the Practice, Springer Berlin Heidelberg, 2015.

[26] R. Krishnan, Electric motor drives, Upper Saddle River: Prentice Hall, 2001.

[27] P. Brandstetter and M. Kuchar, "Rotor flux estimation using voltage model of induction motor," in *2015 16th International Scientific Conference on Electric Power Engineering (EPE)*, 2015, pp. 246-250.

[28] J. Bauer, "Vektorová regulace [lecture]," Czech Technical University in Prague, Prague, 2021.

[29] J. Javůrek, Regulace moderních elektrických pohonů, Prague: Grada Publishing, 2003.

[30] J. Yu, T. Zhang and J. Qian, "10 - Modern control methods for the induction motor," in *Electrical Motor Products*, J. Y. a. T. Z. a. J. Qian, Ed., Woodhead Publishing, 2011, pp. 147-172.

[31] G. Kohlrusz and D. Fodor, "Comparison of Scalar and Vector Control Strategies of Induction Motors," *Hungarian Journal of Industry and Chemistry,* vol. 39, no. 2, p. 265–270, 2011.

[32] E. G. Strangas, "4 - Fault diagnosis and failure prognosis of electrical drives," in *Fault Diagnosis and Prognosis Techniques for Complex Engineering Systems*, H. Karimi, Ed., Academic Press, 2021, pp. 127-180.

[33] A. M. Trzynadlowski, "8 - Direct torque and flux control," in *Control of Induction Motors*, Engineering ed., A. M. Trzynadlowski, Ed., San Diego, Academic Press, 2001, pp. 137-157.

[34] P. Stejskal, "Modulační techniky pro víceúrovňové," Master's Thesis, Czech Technical University in Prague, Prague, 2015.

[35] S. Strobl, "SVPWM vs SPWM modulation techniques," Imperix Ltd, 27 09 2021. [Online]. Available: https://imperix.com/doc/implementation/svpwm-vs-spwm-modulation-techniques. [Accessed 06 - 03 - 2022].

[36] S.-H. Kim, "Chapter 7 - Pulse width modulation inverters," in *Electric Motor Control*, S. Kim, Ed., Elsevier, 2017, pp. 265-340.

[37] K. H. Bhalodi and P. Agrawal, "Space Vector Modulation with DC-Link Voltage Balancing Control for Three-Level Inverters," in *2006 International Conference on Power Electronic, Drives and Energy Systems*, 2006, pp. 1-6.

[38] N. Celanovic and D. Boroyevich, "A comprehensive study of neutral-point voltage balancing problem in three-level neutral-point-clamped voltage source PWM inverters," *IEEE Transactions on Power Electronics,* vol. 15, no. 2, pp. 242-249, 2000.

[39] A. Kocalmis and S. Sunter, "Simulation of a Space Vector PWM Controller For a Three-Level Voltage-Fed Inverter Motor Drive," in *IECON 2006 - 32nd Annual Conference on IEEE Industrial Electronics*, 2006, pp. 1915-1920.

[40] M. Miskiewicz and A. Johannesen, "A three-level Space Vector Modulation strategy for two-level parallel inverters," Master's Thesis, Institute of Energy Technology, 2009.

[41] J. Pou, R. Pindado, D. Boroyevich and P. Rodriguez, "Evaluation of the low-frequency neutral-point voltage oscillations in the three-level inverter," *IEEE Transactions on Industrial Electronics,* vol. 52, no. 6, pp. 1582-1588, 2005.

Appendix A Duty cycles of all sectors

Table 4 Duty cycles of the positive switching sequence

		Phase A	Phase B	Phase C
Sector 1	Region 1	$T_1+T_2+T_0/2$	$T_2+T_0/2$	$T_0/2$
	Region 2	$T_1+T_2/2+T_0$	$T_2/2$	$T_1+T_2/2$
	Region 3	$T_1/2+T_2+T_0$	$T_1/2+T_0$	$T_1/2$
	Region 4	$T_1+T_2/2+T_0$	$T_1+T_2/2$	$T_2/2$
Sector 2	Region 1	$T_2+T_0/2$	$T_1+T_2+T_0/2$	$T_0/2$
	Region 2	$T_2/2$	$T_1+T_2/2+T_0$	$T_1+T_2/2$
	Region 3	$T_1+T_2/2$	$T_1+T_2/2+T_0$	$T_2/2$
	Region 4	$T_1/2+T_0$	$T_1/2+T_2+T_0$	$T_1/2$
Sector 3	Region 1	$T_0/2$	$T_1+T_2+T_0/2$	$T_2+T_0/2$
	Region 2	$T_1+T_2/2$	$T_1+T_2/2+T_0$	$T_2/2$
	Region 3	$T_1/2$	$T_1/2+T_2+T_0$	$T_1/2+T_0$
	Region 4	$T_2/2$	$T_1+T_2/2+T_0$	$T_1+T_2/2$
Sector 4	Region 1	$T_0/2$	$T_2+T_0/2$	$T_1+T_2+T_0/2$
	Region 2	$T_1+T_2/2$	$T_2/2$	$T_1+T_2/2+T_0$
	Region 3	$T_2/2$	$T_1+T_2/2$	$T_1+T_2/2+T_0$
	Region 4	$T_1/2$	$T_1/2+T_0$	$T_1/2+T_2+T_0$
Sector 5	Region 1	$T_2+T_0/2$	$T_0/2$	$T_1+T_2+T_0/2$
	Region 2	$T_2/2$	$T_1+T_2/2$	$T_1+T_2/2+T_0$
	Region 3	$T_1/2+T_0$	$T_1/2$	$T_1/2+T_2+T_0$
	Region 4	$T_1+T_2/2$	$T_2/2$	$T_1+T_2/2+T_0$
Sector 6	Region 1	$T_1+T_2+T_0/2$	$T_0/2$	$T_2+T_0/2$
	Region 2	$T_1+T_2/2+T_0$	$T_1+T_2/2$	$T_2/2$
	Region 3	$T_1+T_2/2+T_0$	$T_2/2$	$T_1+T_2/2$
	Region 4	$T_1/2+T_2+T_0$	$T_1/2$	$T_1/2+T_0$

Table 5 Duty cycles of the positive shift

		Phase A	Phase B	Phase C
Sector 1	Region 1	$T_1+T_2+T_0$	$T_1+T_2+T_0$	$T_1+T_2+T_0$
	Region 2	$T_1+T_2+T_0$	$T_1+T_2+T_0$	0
	Region 3	$T_1+T_2+T_0$	0	0
	Region 4	$T_1+T_2+T_0$	$T_1+T_2+T_0$	0
Sector 2	Region 1	$T_1+T_2+T_0$	$T_1+T_2+T_0$	$T_1+T_2+T_0$
	Region 2	$T_1+T_2+T_0$	$T_1+T_2+T_0$	0
	Region 3	$T_1+T_2+T_0$	$T_1+T_2+T_0$	0

	Region 4	0	$T_1+T_2+T_0$	0
Sector 3	Region 1	$T_1+T_2+T_0$	$T_1+T_2+T_0$	$T_1+T_2+T_0$
	Region 2	0	$T_1+T_2+T_0$	$T_1+T_2+T_0$
	Region 3	0	$T_1+T_2+T_0$	0
	Region 4	0	$T_1+T_2+T_0$	$T_1+T_2+T_0$
Sector 4	Region 1	$T_1+T_2+T_0$	$T_1+T_2+T_0$	$T_1+T_2+T_0$
	Region 2	0	$T_1+T_2+T_0$	$T_1+T_2+T_0$
	Region 3	0	$T_1+T_2+T_0$	$T_1+T_2+T_0$
	Region 4	0	0	$T_1+T_2+T_0$
Sector 5	Region 1	$T_1+T_2+T_0$	$T_1+T_2+T_0$	$T_1+T_2+T_0$
	Region 2	$T_1+T_2+T_0$	0	$T_1+T_2+T_0$
	Region 3	0	0	$T_1+T_2+T_0$
	Region 4	$T_1+T_2+T_0$	0	$T_1+T_2+T_0$
Sector 6	Region 1	$T_1+T_2+T_0$	$T_1+T_2+T_0$	$T_1+T_2+T_0$
	Region 2	$T_1+T_2+T_0$	0	$T_1+T_2+T_0$
	Region 3	$T_1+T_2+T_0$	0	$T_1+T_2+T_0$
	Region 4	$T_1+T_2+T_0$	0	0

Table 6 Duty cycles for the negative switching sequence

		Phase A	Phase B	Phase C
Sector 1	Region 1	$T_1/2+T_0$	$T_1/2+T_2+T_0$	$T_1/2$
	Region 2	$T_1/2+T_2+T_0$	$T_1/2+T_0$	$T_1/2$
	Region 3	$T_1+T_2/2+T_0$	$T_1+T_2/2$	$T_2/2$
	Region 4	$T_2+T_0/2$	$T_1+T_2+T_0/2$	$T_0/2$
Sector 2	Region 1	$T_1/2+T_2+T_0$	$T_1/2+T_0$	$T_1/2$
	Region 2	$T_1+T_2/2$	$T_1+T_2/2+T_0$	$T_2/2$
	Region 3	$T_1/2+T_0$	$T_1/2+T_2+T_0$	$T_1/2$
	Region 4	$T_0/2$	$T_1+T_2+T_0/2$	$T_2+T_0/2$
Sector 3	Region 1	$T_1/2$	$T_1/2+T_0$	$T_1/2+T_2+T_0$
	Region 2	$T_1/2$	$T_1/2+T_2+T_0$	$T_1/2+T_0$
	Region 3	$T_2/2$	$T_1+T_2/2+T_0$	$T_1+T_2/2$
	Region 4	$T_0/2$	$T_2+T_0/2$	$T_1+T_2+T_0/2$
Sector 4	Region 1	$T_1/2$	$T_1/2+T_2+T_0$	$T_1/2+T_0$
	Region 2	$T_2/2$	$T_1+T_2/2$	$T_1+T_2/2+T_0$
	Region 3	$T_1/2$	$T_1/2+T_0$	$T_1/2+T_2+T_0$
	Region 4	$T_2+T_0/2$	$T_0/2$	$T_1+T_2+T_0/2$
Sector 5	Region 1	$T_1/2+T_2+T_0$	$T_1/2$	$T_1/2+T_0$
	Region 2	$T_1/2+T_0$	$T_1/2$	$T_1/2+T_2+T_0$
	Region 3	$T_1+T_2/2$	$T_2/2$	$T_1+T_2/2+T_0$

	Region 4	$T_1+T_2+T_0/2$	$T_0/2$	$T_2+T_0/2$
Sector 6	Region 1	$T_1/2+T_0$	$T_1/2$	$T_1/2+T_2+T_0$
	Region 2	$T_1+T_2/2+T_0$	$T_2/2$	$T_1+T_2/2$
	Region 3	$T_1/2+T_2+T_0$	$T_1/2$	$T_1/2+T_0$
	Region 4	$T_1/2+T_0$	$T_1/2+T_2+T_0$	$T_1/2$

Table 7 Duty cycles for the negative shift

		Phase A	Phase B	Phase C
Sector 1	Region 1	$T_1+T_2+T_0$	$T_1+T_2+T_0$	$T_1+T_2+T_0$
	Region 2	$T_1+T_2+T_0$	$T_1+T_2+T_0$	0
	Region 3	$T_1+T_2+T_0$	0	0
	Region 4	$T_1+T_2+T_0$	$T_1+T_2+T_0$	0
Sector 2	Region 1	$T_1+T_2+T_0$	$T_1+T_2+T_0$	$T_1+T_2+T_0$
	Region 2	$T_1+T_2+T_0$	$T_1+T_2+T_0$	0
	Region 3	$T_1+T_2+T_0$	$T_1+T_2+T_0$	0
	Region 4	0	$T_1+T_2+T_0$	0
Sector 3	Region 1	$T_1+T_2+T_0$	$T_1+T_2+T_0$	$T_1+T_2+T_0$
	Region 2	0	$T_1+T_2+T_0$	$T_1+T_2+T_0$
	Region 3	0	$T_1+T_2+T_0$	0
	Region 4	0	$T_1+T_2+T_0$	$T_1+T_2+T_0$
Sector 4	Region 1	$T_1+T_2+T_0$	$T_1+T_2+T_0$	$T_1+T_2+T_0$
	Region 2	0	$T_1+T_2+T_0$	$T_1+T_2+T_0$
	Region 3	0	$T_1+T_2+T_0$	$T_1+T_2+T_0$
	Region 4	0	0	$T_1+T_2+T_0$
Sector 5	Region 1	$T_1+T_2+T_0$	$T_1+T_2+T_0$	$T_1+T_2+T_0$
	Region 2	$T_1+T_2+T_0$	0	$T_1+T_2+T_0$
	Region 3	0	0	$T_1+T_2+T_0$
	Region 4	$T_1+T_2+T_0$	0	$T_1+T_2+T_0$
Sector 6	Region 1	$T_1+T_2+T_0$	$T_1+T_2+T_0$	$T_1+T_2+T_0$
	Region 2	T1+T2+T0	0	T1+T2+T0
	Region 3	T1+T2+T0	0	T1+T2+T0
	Region 4	T1+T2+T0	0	0

Appendix B MATLAB code

```
clear all; % clear Workspace
clc; % clear Command Window
%-------------------------------------------------
%   Machine parameters
Pn = 2250*746; % nominal power [W]
cosphin = 0.8; % power factor [-]
Sn = Pn/cosphin; % nominal apparent power
Vn = 2.4e3; % nominal line-line voltage [V]
fn = 60; % nominal frequency [Hz]
In = Pn/(sqrt(3)*Vn*cosphin); % nominal rms current [A]
nn = 1794; % nominal speed [rpm]
pp = 2; % number of pole pairs [-]
Rs = 0.029; % stator resistance [Ω]
Rr = 0.022; % rotor resistance [Ω]
Lls = 0.226/(2*pi*fn); % stator leakage inductance [H]
Llr = 0.226/(2*pi*fn); % rotorleakage inductance [H]
Lm = 13.04/(2*pi*fn); % mutual inductance [H]
Ls = Lls+Lm; % stator inductance [H]
Lr = Llr+Lm; % rotor inductance [H]
J = 63.87; % moment of inertia [kg m2]
wn = nn*2*pi/60; % nominal speed [rad/s]
Tn = 8935; % nominal torque [N m]
B = 0.005879; % friction koefficient [N m/rad/s]
%-------------------------------------------------
%   Additional parameters
VRef = Vn/sqrt(3)*sqrt(2); % line-to-neutral voltage amplitude [V]
V_DC = VRef*sqrt(3); % DC-bus voltage [V]
VRec = VRef; % line-to-neutral voltage amplitude for rectifier's supply [V]
Ts = 1e-4; % modulation period [sec]
Tp = Ts/2; % carrier wave peak [sec]
K = 2/3; % Clarke transformation constant [-]
r = 0.5; % PWM carrier waves ratio [-]
dVper = 1/1000; % allowed tolerance between inputs in "Approx. equal" block [-]
%-------------------------------------------------
%   Tables matrixes
level_merg = [1 0; 2 3]; % PWM carrier waves merging matrix; 0 ~ -1, 1 ~ 0, 2 ~ +1, 3 ~↙
ERR; located in "Signal calculation" block
gate_sig = [[0 0 1 0];[0 1 1 0];[1 1 0 0];[1 0 0 0]]; % PWM gates signal matrix; located↙
in "Signal calculation NPC" block
balancing = cat(3, [0 1; 0 1], [0 3; 0 3]); % balancing matrix; located in "Balancing↙
table" block
minimA = [[1 0];[1 1];[0 1];[0 0]]; % matrix for minimizing dV between C1 & C2, for phase↙
A; located in "Minimizing dVA" block
minimBC = [[0 0];[1 0];[1 1];[0 1]]; % matrix for minimizing dV between C1 & C2, for↙
phase B, C; located in "Minimizing dVBC" block
%-------------------------------------------------
%   Simscape parameters for Rectifier and NPC
Rcset = 3e0; % parallel resistance of C1, C2 [Ω]
Rchar = 1.1e-1; % resistance of charging circuit [Ω]
Lchar = 3e-2; % inductance of charging circuit [H]
Cset = 1e-1; % capacitance of C1, C2 [F]
```

Fig. 37 MATLAB code used for simulation part 1

```
C_diff = 1; % allowed tolerance between C1 & C2 [-]
C1ini = V_DC/2; % initial voltage of C1 [F]
C2ini = V_DC/2; % initial voltage of C2 [F]
%--------------------------------------------------
%   Calculation of saturation limits for flux & speed regulators
Inmax = In*sqrt(2); % current amplitude
phi = acos(cosphin); % power factor angle
psisn = VRef/wn; % nominal stator flux linkage
psisn = sqrt((VRef-Rs*Inmax*cosphin)^2+(Rs*Inmax*sin(phi))^2)/(2*pi*fn); % nominal stator↙
flux linkage
Phi = asin((Rs*Inmax*sin(phi))/(2*pi*fn*psisn)); % angle between phasors Us & psisn
psisnRe = psisn*cos(Phi); % real part of psisn
psisnIm = psisn*sin(Phi); % imaginary part of psisn
IsnRe = In*sin(phi); % real part of Isn (In)
IsnIm = In*cos(phi); % imaginary part of Isn (In)
sigma = 1-Lm^2/(Ls*Lr); % leakage factor
psirnRe = Lr/Lm*(psisnRe-sigma*Ls*IsnRe); % real part of psirn
psirnIm = Lr/Lm*(psisnIm-sigma*Ls*IsnIm); % imaginary part of psirn
psirn = sqrt(psirnRe^2+psirnIm^2); % nominal rotor flux linkage
isdn = psirn/Lm; % d-axis component of isn (In)
isqn = sqrt(Inmax^2-isdn^2); % q-axis component of isn (In)
```

Fig. 38 MATLAB code used for simulation part 2